

Major expansion in the human niche preceded out of Africa dispersal

<https://doi.org/10.1038/s41586-025-09154-0>

Received: 19 November 2021

Accepted: 14 May 2025

Published online: 18 June 2025

Open access

 Check for updates

Emily Y. Hallett^{1,2,11}✉, Michela Leonardi^{3,4,11}✉, Jacopo Niccolò Cerasoni^{2,5}, Manuel Will^{6,7}, Robert Beyer³, Mario Krapp³, Andrew W. Kandel⁸, Andrea Manica^{3,11}✉ & Eleanor M. L. Scerri^{2,9,10,11}✉

All contemporary Eurasians trace most of their ancestry to a small population that dispersed out of Africa about 50,000 years ago (ka)^{1–9}. By contrast, fossil evidence attests to earlier migrations out of Africa^{10–15}. These lines of evidence can only be reconciled if early dispersals made little to no genetic contribution to the later, major wave. A key question therefore concerns what factors facilitated the successful later dispersal that led to long-term settlement beyond Africa. Here we show that a notable expansion in human niche breadth within Africa precedes this later dispersal. We assembled a pan-African database of chronometrically dated archaeological sites and used species distribution models (SDMs) to quantify changes in the bioclimatic niche over the past 120,000 years. We found that the human niche began to expand substantially from 70 ka and that this expansion was driven by humans increasing their use of diverse habitat types, from forests to arid deserts. Thus, humans dispersing out of Africa after 50 ka were equipped with a distinctive ecological flexibility among hominins as they encountered climatically challenging habitats, providing a key mechanism for their adaptive success.

Genetic evidence, including patterns of interbreeding with Eurasian hominins, indicates that all contemporary human populations outside Africa derive most of their ancestry from a worldwide expansion that began approximately 50 ka (refs. 1–9). However, the fossil record shows that earlier dispersals also occurred^{10–16}. These dispersals out of Africa probably took place during repeated humid episodes within the Saharo-Arabian arid belt, most notably during the Last Interglacial, approximately 125 ka (refs. 10,17). An important question, therefore, concerns why these earlier dispersals were not successful enough to contribute any detectable genetic ancestry of non-African populations today, with early *Homo sapiens* failing to establish long-term viable populations in areas beyond Africa.

Researchers have proposed a range of explanations for the late dispersal of modern humans from Africa. Studies have considered that abrupt climate change in Africa¹⁸ and large shifts in human cognition, technology and subsistence permitted the development of new ‘niche-broadening’ innovations, such as the distinctly human ability to communicate symbolically or develop projectile weaponry^{19–23}. However, complex weaponry has now been shown to have notable time depth in Africa^{24,25} and recurrent markers of symbolic behaviour are present at least during Marine Isotope Stage 5 (MIS 5, 130–71 ka) in both Africa^{26–30} and Southwest Asia^{29,30}. By around 60 ka, the Middle Stone Age/Middle Palaeolithic archaeological record of Northeast Africa and neighbouring regions of Southwest Asia had become rather generic^{31,32}, with no particularly notable, regionally specific shared characteristics.

More broadly, the African archaeological record features complex, nonlinear trajectories of cultural change^{33,34}. These often include long periods of stasis punctuated by relatively brief pulses of innovation in different African regions^{35–41} thousands of years before the advent of Eurasian founder populations^{10,42}. Large, cumulative changes in the archaeological record also post-date the 60–50-ka time frame¹⁰, suggesting that the success of modern human founding populations in Eurasia did not rest on a particular widespread technological innovation or sudden increased cognitive capacity⁴³. More recent studies have focused on a variety of interrelated explanations rooted in demography. In particular, the apparent geographic expansion of Middle Stone Age archaeological sites in Africa 125–50 ka has been considered to reflect a possible growth in population coupled with an expansion inside Africa of an ancestry similar to the major expansion wave^{1,44–46}. This population expansion is also thought to include greater population density⁴⁷ and increases in connectivity through long-distance social networks⁴⁸, all of which may have acted as ‘push’ factors. Building on quantitative studies of niche changes associated with hominin species⁴⁹, and with particular Middle Stone Age lithic industries²², the spatial patterning of sites has also been used to suggest a uniquely human adaptation to a ‘generalist–specialist’ niche⁵⁰. However, none of these hypotheses have been quantitatively assessed on a continental scale and few have been examined in terms of the predictions of suitable theoretical models, risking a proliferation of post-hoc explanations^{51,52}. Because human expansion within and out of Africa can be linked to expansions

¹Department of Anthropology, Loyola University Chicago, Chicago, IL, USA. ²Human Palaeosystems Group, Max Planck Institute of Geoanthropology, Jena, Germany. ³Department of Zoology, University of Cambridge, Cambridge, UK. ⁴Natural History Museum, London, UK. ⁵Department of Biology, Loyola University Chicago, Chicago, IL, USA. ⁶Department of Early Prehistory and Quaternary Ecology, Eberhard Karls University of Tübingen, Tübingen, Germany. ⁷Palaeo-Research Institute, University of Johannesburg, Johannesburg, South Africa. ⁸The Role of Culture in Early Expansions of Humans (ROCEEH), Heidelberg Academy of Sciences and Humanities at Eberhard Karls University of Tübingen, Tübingen, Germany. ⁹Department of Classics and Archaeology, University of Malta, Msida, Malta. ¹⁰Department of Prehistoric Archaeology, University of Cologne, Cologne, Germany. ¹¹These authors contributed equally: Emily Y. Hallett, Michela Leonardi, Andrea Manica, Eleanor M. L. Scerri. ✉e-mail: ehallett2@luc.edu; ml897@cam.ac.uk; am315@cam.ac.uk; scerri@gea.mpg.de

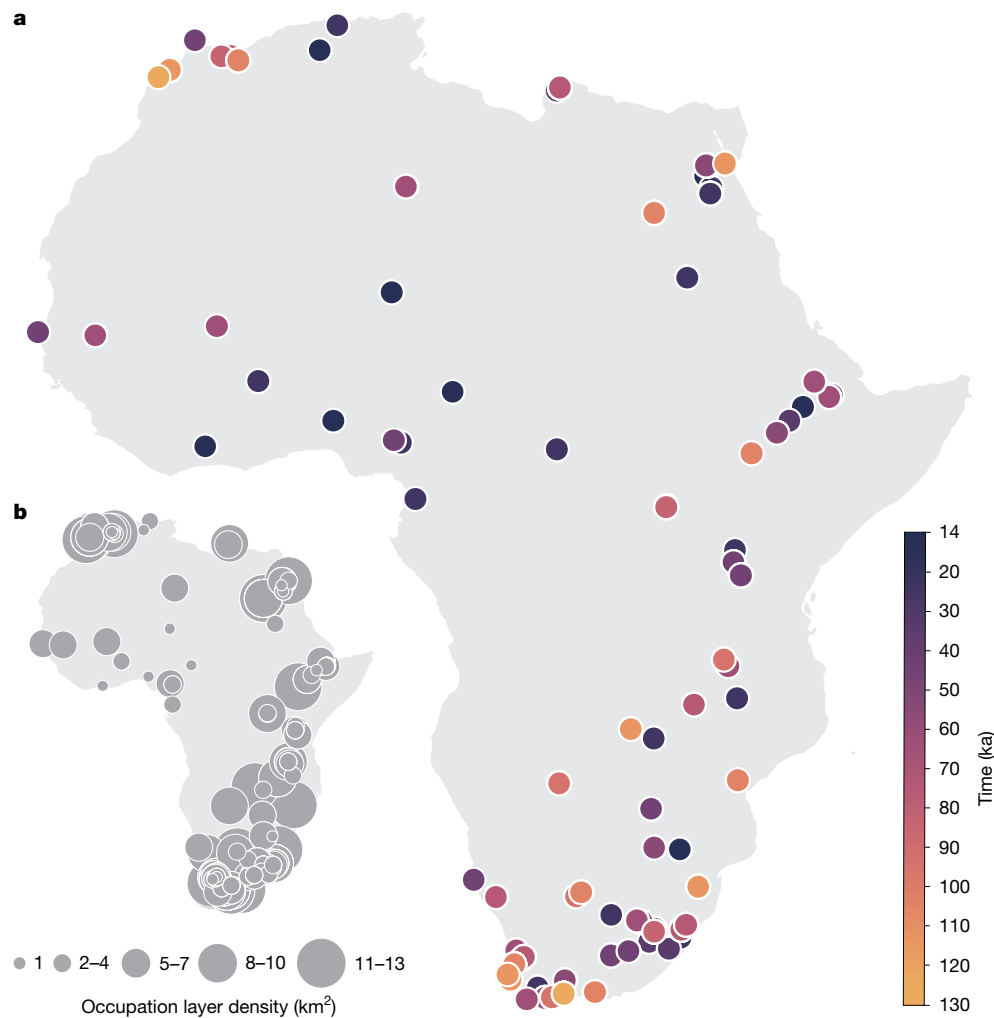


Fig. 1 | Map of dated archaeological sites in Africa. a, Location and time ranges of archaeological sites. **b,** Density of radiometrically dated archaeological layers per square kilometre used in this study (see Supplementary Table 1). The sample size is 479.

in niche breadth under an ideal free distribution⁵³ model, we explored successful out of Africa in terms of expansions of the human niche. As population densities increase, human settlement in more challenging environments becomes profitable. Under such conditions, in which the critical population mass required for successful out of Africa movements is reached and the ecological resilience of humans increases, expansions can occur^{54,55}.

Here we specifically test whether the niche of Pleistocene *H. sapiens* expanded or contracted within Africa before major dispersals out of the continent. We define niche as the ensemble of bioclimatic factors determining where the species can survive and reproduce⁵⁶. To answer this question, we build on previous studies^{22,57–60} and use a SDM approach⁶¹ to measure changes in the breadth of the Pleistocene human niche within Africa. Our results, tested against two different sets of palaeoenvironmental simulations^{62–64}, formally demonstrate that human niche expansion precedes and coincides with successful later dispersal out of Africa.

Testing for the presence of niche change

To reconstruct the human niche in Africa over time, we took a pan-African approach and assembled a comprehensive and curated database of radiometrically dated Pleistocene occupation layers from archaeological sites in the time frame 120–14 ka, excluding any site with an age uncertainty greater than 20,000 years (see Methods for details

on the choice of sites and Supplementary Table 1 for sites included here). For each retained occupation layer (Fig. 1), which represents a confirmed presence, we then extracted reconstructed palaeoclimatic variables and biomes⁶² (based on vegetation simulations with the BIOME4 model) associated with the location and date for a total of 479 radiometrically dated occurrences. We focused on five bioclimatic and vegetation variables that seemed to be the most informative to reconstruct habitat suitability based on our data (see Methods): (1) leaf area index (LAI); (2) temperature annual range (BIO 7); (3) mean temperature of the wettest quarter (BIO 8); (4) mean temperature of the warmest quarter (BIO 10); and (5) precipitation of the wettest quarter (BIO 16). Because of the limited amount of data for each specific biome, the vegetation simulations from BIOME4 were combined into three main classes: forest, savannah and desert (see Methods and Supplementary Table 4). We used two sets of palaeoclimatic simulations based on: (1) the Hadley Centre Coupled Model, version 3 (HadCM3 (ref. 62)), with results presented in the main text, and (2) the Transient Community Earth System Model (PCESM^{63,64}), with results shown in Extended Data Fig. 8a. Although the two sets of simulations have a high degree of correlation, the magnitude in fluctuations for both temperature and precipitation differs through time and space (Extended Data Fig. 8a); despite these discrepancies, all of the key results are qualitatively robust to the palaeoclimate model used.

To reconstruct the human niche over time, we used a SDM approach fitted to the five bioclimatic variables. Biome classes were not used as

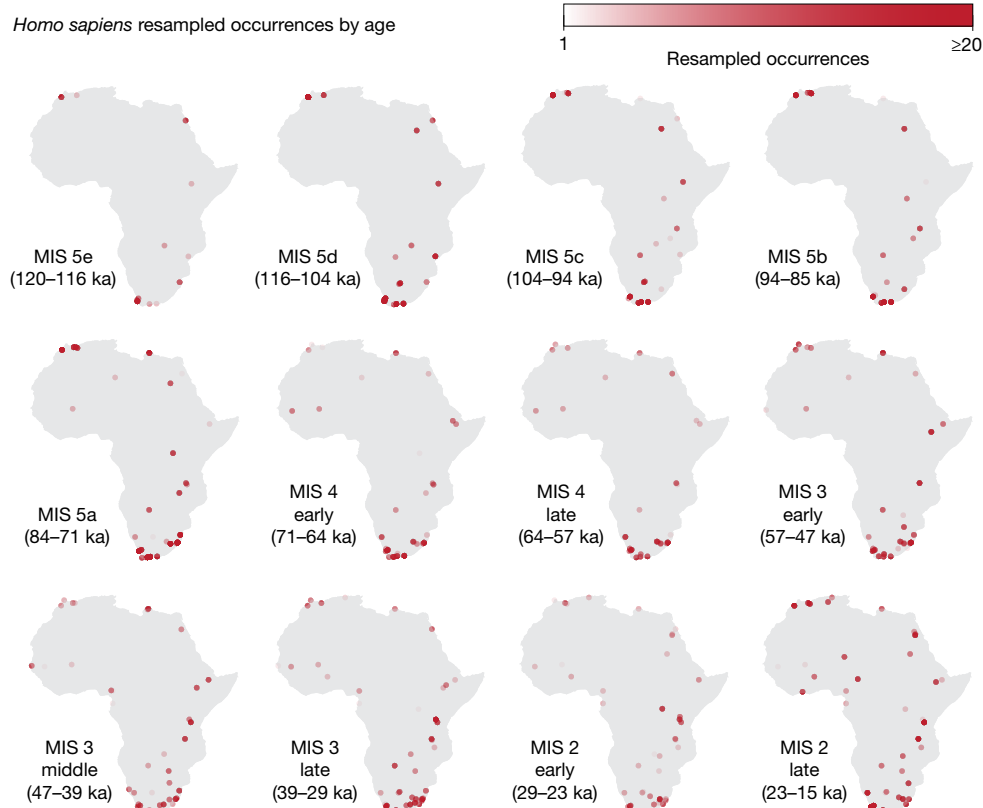


Fig. 2 | *Homo sapiens* resampled occurrences by MIS. To handle chronological uncertainty of archaeological layers, we resampled dates from the appropriate ranges: the saturation of the points indicates the number of resamples that were attributed to a given location for each MIS (darker points come from layers with

low uncertainty for which most dates fall within the same MIS; lighter points represent layers with high uncertainty for which resamples are spread among several MISs). Details of the resampling approach and chronological subdivisions within MIS 4, MIS 3 and MIS 2 are described in Methods.

inputs for the SDMs but only to characterize the environment of cells predicted as habitable by the models. Conventionally, niche changes are tested by fitting SDMs to different time periods and comparing the inferred niches. However, data for Pleistocene humans are very sparse and it would not be possible to create several time slices with enough occurrences. Instead, we use generalized additive models (GAMs) to fit the full time series as a single dataset⁶⁵. With this approach, it is possible to formally test for changes in the niche over time by comparing a GAM in which the effect of each environmental variable in predicting occurrences is constant through time (fixed-niche GAM) against a GAM in which the effect is allowed to vary (changing-niche GAM; formally, by fitting an interaction between each predictor and time; see Methods).

The number of dated archaeological layers in our dataset varies with time, with an increase in abundance towards more recent periods (Extended Data Fig. 1a). This pattern probably results from increased chances of preservation in the more recent past, thus constituting a form of sampling bias that could distort the results. To avoid such a bias, we randomly subsampled the observations to generate a homogeneous distribution in the number of occurrences through time (Extended Data Fig. 1b). We repeated this process 100 times to generate several ‘standard-effort datasets’ to explore the stochastic effect of such subsampling (Fig. 2). We took into account the chronological uncertainty associated with each radiometric date as follows: in each of these datasets, we associated each occurrence with a date sampled from its whole available chronological range (following a normal distribution around the mean). Finally, for each standard-effort dataset, we then quantified the background distribution of the climate variables against the occurrences, sampling 200 random locations matched in time for each occurrence. Next, we fitted a fixed-niche GAM

and a changing-niche GAM to each set of standard-effort occurrences coupled with the associated pseudo-absence points, giving us 100 repeats of our analysis. Formal model comparisons using the Akaike information criterion (AIC) strongly supported the changing-niche GAM in 91 of 100 repeats (see Methods). To understand the changes in the niche detected by the model, we combined repeats into an ensemble⁶⁶; specifically, we combined repeats with the AIC supporting a changing-niche GAM and a Boyce continuous index (BCI; a measure of goodness of fit for presence-only data)⁶⁷ larger than 0.7 and investigated changes over time. We also created an ensemble from the repeats with AIC < 2 (hence not substantially supporting a changing-niche model) using the fixed-niche GAMs, which provides us with a null model of the changes owing to climatic fluctuations over time in the absence of any niche change. A qualitatively similar pattern can be observed on the same analyses performed using the PCESM palaeoclimatic simulations⁶³.

Geographic range expanded 70 ka

The ensemble of changing-niche GAMs showed a substantial increase in the habitable geographic range of Pleistocene humans within Africa over time (Fig. 3). The most notable increase was in West, Central and North Africa beginning roughly 70 ka at the onset of MIS 4. This large increase in geographic range around 70 ka was followed by a range expansion encompassing most of Africa beginning about 29 ka, during MIS 2 (Fig. 3). These changes were the result of niche expansion, as the fixed-niche GAM predicted a relatively stable and extensive inhabitation of the whole continent (Extended Data Fig. 2). Qualitatively similar results were obtained performing the same analyses with the PCESM climate simulations (Extended Data Figs. 8b and 10).

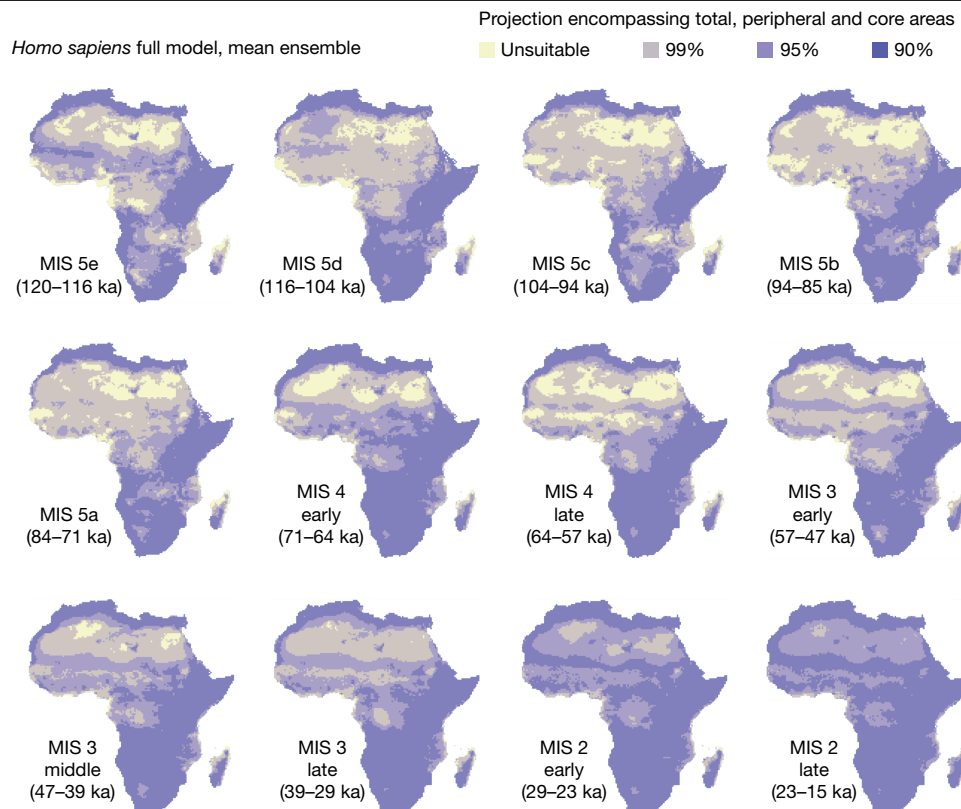


Fig. 3 | Projection of habitat suitability through time for the changing-niche model. Mean ensemble; see Methods. Yellow represents unsuitable areas and the purple colours represent increased suitability from lighter to darker shades. These are calculated as total, peripheral and core areas, encompassing 99%, 95% and 90% of archaeological occurrences, respectively.

The maps for each MIS are produced by calculating the mean of the habitat suitability for each individual cell within the time slices of interest. Chronological subdivisions of MIS 4, MIS 3 and MIS 2 are described in the Methods. The climate used is that of Beyer et al.⁶² with added Heinrich events. See Extended Data Fig. 8b for equivalent results using PCESM^{63,64}.

Changes in niche breadth

To better understand the relationship between these changes in geographic range and the realized niche breadth as defined by the ensemble of changing-niche GAMs (Fig. 4a), we investigated the changes in niche breadth for each biome class under both the changing-niche and the fixed-niche models. We created a principal component analysis of the environmental variables used in the GAMs, pooling over all time steps, to generate a synthetic 2D space that describes climatic variability over the period of interest. For each time step, we then measured the area of a kernel fitted over the locations that were predicted as suitable by the respective model in each biome class (Fig. 4b). We also explored the interaction plots (that is, the partial effects of the interaction between each bioclimatic variable and time) of the ensemble of changing-niche GAMs (Extended Data Fig. 3) to understand the exact changes in the niche, as these represent the (theoretical) full niche and are not affected by the availability of different climatic conditions. Figure 4b shows the size of the realized niche for each biome within Africa, allowing the relationship between humans and climate to change (changing-niche model), whereas Extended Data Fig. 4 compares (for both palaeoclimatic simulations used) this pattern with the plot assuming this relationship to be constant (fixed-niche model). As a result, the latter represents how human distribution would have changed only following climatic fluctuations.

As shown in Fig. 4b, after fluctuations around a relatively stable level up to MIS 5a, the potential use of savannah and forest started to increase steadily between MIS 5a and MIS 4. The increase was not linked to an increase in availability of those habitats, as it was not reproduced by the fixed-niche GAM (see Extended Data Fig. 4a for an equivalent plot to Fig. 4b). Rather, use of areas in which the wettest quarter was both

warmer (BIO 8) and had greater precipitation (BIO 16; see Extended Data Fig. 3) increased, thus expanding the niche progressively into the forests. The use of deserts was more variable, in part because of fluctuations in the degree of aridity of deserts available. During wetter periods, we found an increase in the niche space of deserts that were suitable for human habitation, as they were less extreme in their climatic characteristics. We observe this effect in the reconstructed realized niche area of the fixed-niche GAM, in which changes through time are only linked to climatic changes affecting available climate conditions (see Extended Data Fig. 4a). The key difference between the changing-niche and fixed-niche GAMs is that, in the former, after a peak during early MIS 5a owing to more favourable climate, deserts remain in greater use than during previous, less favourable dips. This stable expansion into the desert is then maintained until MIS 3, when we see another progressive increase in the use of desert habitats. This was not seen in the fixed-niche GAM. Mechanistically, the increased use of deserts was underpinned by an increased use of regions with larger annual temperature ranges (BIO 7 in Extended Data Fig. 3) and a progressive increase in the ability to survive in areas with low LAI (that is, with sparse vegetation; LAI in Extended Data Fig. 3). Although slightly muted, the same patterns were observed when repeating the analyses using the biome classes based on PCESM⁶⁴ (Extended Data Figs. 4b and 9).

Discussion

Our results show that the human niche progressively expanded to include more habitat types beginning around 70 ka and that this expansion peaked at about 50 ka, coinciding with successful dispersals out of Africa. A second expansion was observed starting approximately 29 ka;

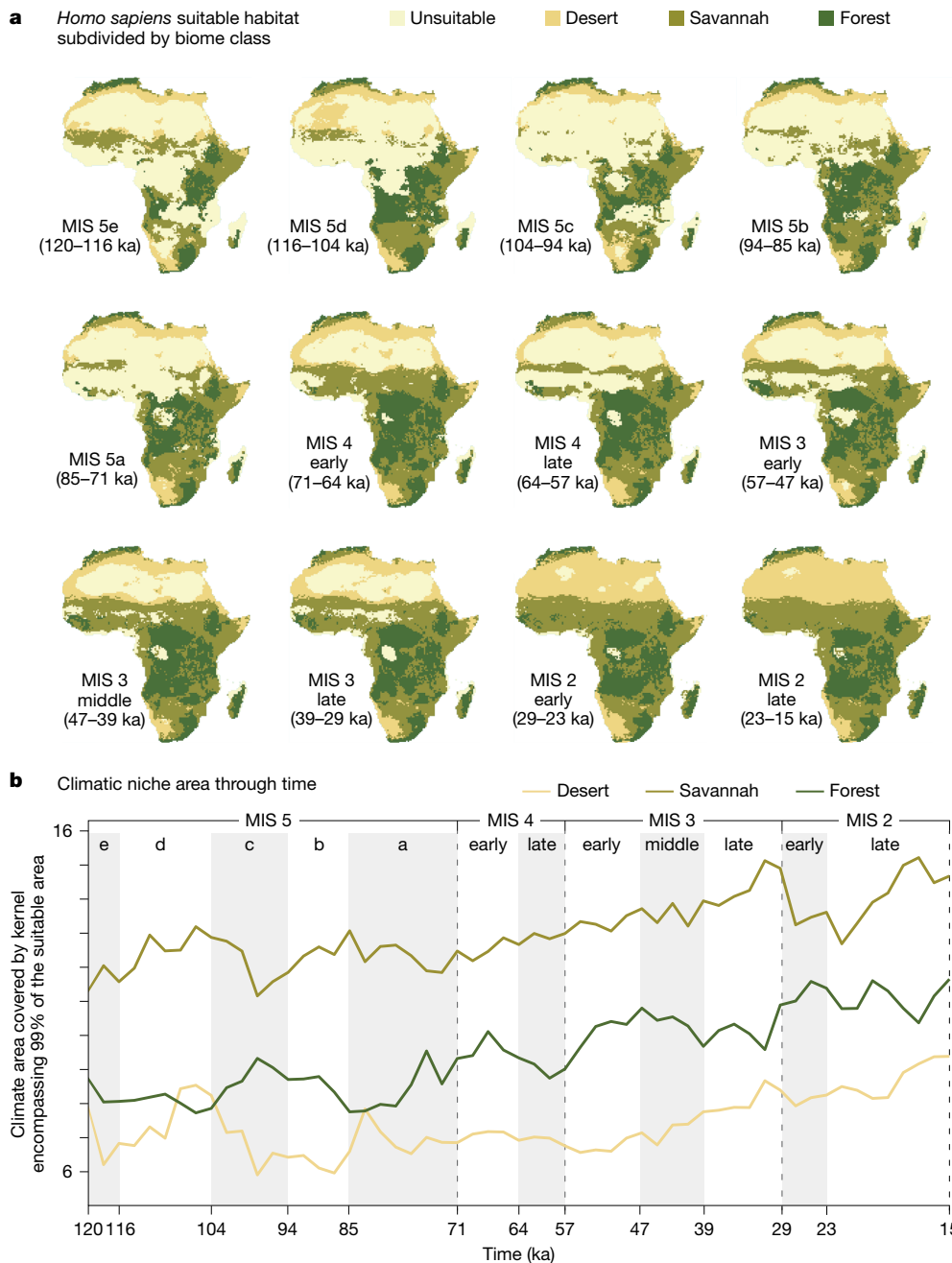


Fig. 4 | *Homo sapiens* suitable habitat and climatic niche area through time. **a**, *Homo sapiens* suitable habitat (combined core and peripheral areas) subdivided by biome class (desert, savannah and forest). **b**, Climatic niche area through time. The niche area is calculated on the plot of the first two principal

components of the climatic variables by estimating the 2D 99% kernel encompassing the suitable cells (combined core and peripheral areas) for each biome class. Equivalent results using PCESM^{63,64} are shown in Extended Data Fig. 4a.

by MIS 2, humans occupied all African regions and ecosystems, with terminal Pleistocene societies engaging with a range of new behaviours, including semi-sedentism⁶⁸, evidence of persistent macroscale social networking⁶⁹ and increased territoriality and interpersonal violence⁷⁰. Our findings are consistent using two different and independently developed sets of palaeoenvironmental simulations. The expansion of the human niche beginning around 70 ka in Africa is driven by a gradual increase in human preference for forest and desert biomes, allowing them to expand into regions that were previously rarely populated: (1) forests of West Africa, (2) forests of Central Africa and, eventually, (3) arid Saharan regions and semi-arid Sahelian regions of North Africa. This increased ability to adapt to new habitats, ranging from the extremes of equatorial forests to arid deserts, would have allowed

these populations of humans the ecological flexibility to tackle a range of new environmental conditions encountered during the expansion out of Africa, allowing them to succeed where earlier migrations out of Africa had previously faltered. The expansion of the human niche in Africa starting around 70 ka, therefore, offers an explanation for the successful worldwide expansion of human populations about 50 ka and is consistent with predictions informed by the ideal free distribution about the consequences of population expansions.

These results also offer insights into changes in the archaeological record between approximately 70 and 50 ka, a time when diverse regions feature distinctive cultural trajectories (see Supplementary Information). In particular, ecosystem engineering through widespread burning⁷¹, water storage technology^{72,73} and expanded diet breadth⁷⁴ have

been previously documented in Africa broadly within this time frame and slightly before. These findings may reflect behavioural preconditions and manifestations of the expansion of the human niche into new habitats. It is important to stress that our pan-African results do not imply a unique, unified process over the whole continent. It is indeed more likely that it is linked to a few specific cultural complexes. More research must be carried out to unravel what drove the changes that we observe.

We emphasize that, although we document a niche expansion, this does not necessarily reflect an increase in overall population size and it may not be possible to distinguish between the effects of population size increase versus increases in density within reduced niche space⁴⁷. For example, the new human niche in arid regions was unlikely to have sustained large or stable population sizes owing to low carrying capacity⁷⁵. Instead, the expansion of the human niche indicates that humans were able to move among several habitats and locations, probably increasing the encounter rate between different groups over time. If this were the case, it may explain why the constellation of features that define humans today became fixed in individuals between 100 and 50 ka (ref. 42). It would also provide independent support for the hypothesis that there could have been an expansion inside Africa of an ancestry that is similar to the one that expanded into Eurasia after about 60 ka (refs. 44,45).

The period roughly 70–50 ka is climatically complex. Although the Heinrich Event 6 brings an overall cooler and drier spell owing to the weakening of the Atlantic Meridional Overturning Circulation⁷⁶, the magnitude of this effect differs across regions of Africa. Notably, the proxy record points to repeated shifts between dry and wet spells⁷⁷, with suggestions of a broader humid period that might have affected a large part of the continent following Heinrich Event 6 (ref. 78). Our runs of HadCM3 (combining Beyer et al.⁶² and Armstrong et al.⁷⁹) capture this temporal and spatial heterogeneity (Extended Data Fig. 8a); in PAGESM^{63,64}, which does not explicitly include Heinrich Event 6, the pattern is more muted (Extended Data Fig. 8a). The impact of Heinrich Event 6 for human evolution has mostly been framed in terms of its role in dispersals out of Africa. It has been argued that the aridification of Northern and Eastern Africa might have acted as a push event favouring migrations of humans out of Africa⁸⁰; however, it should also be noted that, because of the cooling effect and its heterogeneous impact, this period potentially provided corridors that might have favoured movement out of the continent⁸¹. A similar argument can be made for the onset of MIS 2 around 29 ka, when a period of heterogeneous aridification prompted a further move into more arid habitats. Given our results, it is plausible that the instability of climate in these periods might have favoured the evolution of a broader niche in humans, further enhancing their ability to cope with the diverse habitats that distinguish the genus *Homo*⁶⁴.

By modelling the human niche within Africa from 120 to 14 ka, we show that successful expansion into Eurasia and the long-term establishment of populations there were part of a process that fundamentally started within Africa. Essentially, we document the inception of an unquestionably African process originating 70 ka that has resulted in today's unparalleled human ecological plasticity. Our results, therefore, provide a new basis for understanding and investigating our species' global dispersal.

Online content

Any methods, additional references, Nature Portfolio reporting summaries, source data, extended data, supplementary information, acknowledgements, peer review information; details of author contributions and competing interests; and statements of data and code availability are available at <https://doi.org/10.1038/s41586-025-09154-0>.

1. Bergström, A., Stringer, C., Hajdinjak, M., Scerri, E. M. L. & Skoglund, P. Origins of modern human ancestry. *Nature* **590**, 229–237 (2021).
2. Fu, Q. et al. The genetic history of Ice Age Europe. *Nature* **534**, 200–205 (2016).

3. Seguin-Orlando, A. et al. Genomic structure in Europeans dating back at least 36,200 years. *Science* **346**, 1113–1118 (2014).
4. Fu, Q. et al. Genome sequence of a 45,000-year-old modern human from western Siberia. *Nature* **514**, 445–449 (2014).
5. Sikora, M. et al. Ancient genomes show social and reproductive behavior of early Upper Paleolithic foragers. *Science* **358**, 659–662 (2017).
6. Sikora, M. et al. The population history of northeastern Siberia since the Pleistocene. *Nature* **570**, 182–188 (2019).
7. Yang, M. A. et al. 40,000-year-old individual from Asia provides insight into early population structure in Eurasia. *Curr. Biol.* **27**, 3202–3208 (2017).
8. Sümer, A. P. et al. Earliest modern human genomes constrain timing of Neanderthal admixture. *Nature* **638**, 711–717 (2025).
9. Iasi, L. N. M. et al. Neanderthal ancestry through time: insights from genomes of ancient and present-day humans. *Science* **386**, eadq3010 (2024).
10. Groucutt, H. S. et al. Rethinking the dispersal of *Homo sapiens* out of Africa. *Evol. Anthropol.* **24**, 149–164 (2015).
11. Groucutt, H. S. et al. *Homo sapiens* in Arabia by 85,000 years ago. *Nat. Ecol. Evol.* **2**, 800–809 (2018).
12. Grün, R. et al. U-series and ESR analyses of bones and teeth relating to the human burials from Skhul. *J. Hum. Evol.* **49**, 316–334 (2005).
13. Valladas, H., Merriam, N., Joron, J.-L. & Reyss, J.-L. in *Neanderthals and Modern Humans in Western Asia* (eds Akazawa, T., Aoki, K. & Bar-Yosef, O.) 69–75 (Springer, 1998).
14. Hershkovitz, I. et al. The earliest modern humans outside Africa. *Science* **359**, 456–459 (2018).
15. Harvati, K. et al. Apidima Cave fossils provide earliest evidence of *Homo sapiens* in Eurasia. *Nature* **571**, 500–504 (2019).
16. Freidline, S. E. et al. Early presence of *Homo sapiens* in Southeast Asia by 86–68 kyr at Tam Pa Ling, Northern Laos. *Nat. Commun.* **14**, 3193 (2023).
17. Breeze, P. et al. Palaeohydrological corridors for hominin dispersals in the Middle East ~250–70,000 years ago. *Quat. Sci. Rev.* **144**, 155–185 (2016).
18. Carto, S. L., Weaver, A. J., Hetherington, R., Lam, Y. & Wiebe, E. C. Out of Africa and into an ice age: on the role of global climate change in the late Pleistocene migration of early modern humans out of Africa. *J. Hum. Evol.* **56**, 139–151 (2009).
19. Mellars, P. Why did modern human populations disperse from Africa ca. 60,000 years ago? A new model. *Proc. Natl Acad. Sci.* **103**, 9381–9386 (2006).
20. Klein, R. G. Out of Africa and the evolution of human behavior. *Evol. Anthropol.* **17**, 267–281 (2008).
21. Mellars, P., Gori, K. C., Carr, M., Soares, P. A. & Richards, M. B. Genetic and archaeological perspectives on the initial modern human colonization of southern Asia. *Proc. Natl Acad. Sci.* **110**, 10699–10704 (2013).
22. d'Errico, F. et al. Identifying early modern human ecological niche expansions and associated cultural dynamics in the South African Middle Stone Age. *Proc. Natl Acad. Sci.* **114**, 7869–7876 (2017).
23. d'Errico, F. & Banks, W. E. Identifying mechanisms behind Middle Paleolithic and Middle Stone Age cultural trajectories. *Curr. Anthropol.* **54**, S371–S387 (2013).
24. Wilkins, J., Schoville Benjamin, J., Brown Kyle, S. & Chazan, M. Evidence for early hafted hunting technology. *Science* **338**, 942–946 (2012).
25. Backwell, L. et al. The antiquity of bow-and-arrow technology: evidence from Middle Stone Age layers at Sibudu Cave. *Antiquity* **92**, 289–303 (2018).
26. Bouzouggar, A. et al. 82,000-year-old shell beads from North Africa and implications for the origins of modern human behavior. *Proc. Natl Acad. Sci.* **104**, 9964–9969 (2007).
27. Henshilwood, C., d'Errico, F., Vanhaeren, M., van Niekerk, K. & Jacobs, Z. Middle Stone Age shell beads from South Africa. *Science* **304**, 404 (2004).
28. d'Errico, F., Henshilwood, C., Vanhaeren, M. & van Niekerk, K. *Nassarius kraussianus* shell beads from Blombos Cave: evidence for symbolic behaviour in the Middle Stone Age. *J. Hum. Evol.* **48**, 3–24 (2005).
29. Vanhaeren, M. et al. Middle Paleolithic shell beads in Israel and Algeria. *Science* **312**, 1785–1788 (2006).
30. Steele, T., Álvarez-Fernández, E. & Hallett-Desguez, E. Special Issue: Early personal ornaments: a review of shells as personal ornamentation during the African Middle Stone Age. *PaleoAnthropology* **2019**, 24–51 (2019).
31. Shea, J. J. The Middle Paleolithic of the East Mediterranean Levant. *J. World Prehist.* **17**, 313–394 (2003).
32. Scerri, E. M. L. The North African Middle Stone Age and its place in recent human evolution. *Evol. Anthropol.* **26**, 119–135 (2017).
33. Will, M., Conard, N. J. & Tryon, C. A. in *Modern Human Origins and Dispersal* (eds Sahle, Y., Reyes-Centeno, H. & Bentz, C.) 25–72 (Kerns Verlag, 2019).
34. Scerri, E. M. L. & Will, M. The revolution that still isn't: the origins of behavioral complexity in *Homo sapiens*. *J. Hum. Evol.* **179**, 103358 (2023).
35. Brown, K. S. et al. An early and enduring advanced technology originating 71,000 years ago in South Africa. *Nature* **491**, 590–593 (2012).
36. Brown, K. S. et al. Fire as an engineering tool of early modern humans. *Science* **325**, 859–862 (2009).
37. Henshilwood, C. S. et al. A 100,000-year-old ochre-processing workshop at Blombos Cave, South Africa. *Science* **334**, 219–222 (2011).
38. Clark, J. D. The Middle Stone Age of East Africa and the beginnings of regional identity. *J. World Prehist.* **2**, 235–305 (1988).
39. Tryon, C. A. & Faith, J. T. Variability in the Middle Stone Age of eastern Africa. *Curr. Anthropol.* **54**, S234–S254 (2013).
40. Dibble, H. L. et al. On the industrial attributions of the Aterian and Mousterian of the Maghreb. *J. Hum. Evol.* **64**, 194–210 (2013).
41. Jacobs, Z., Roberts, R. G., Nespoulet, R., El Hajraoui, M. A. & Debénath, A. Single-grain OSL chronologies for Middle Palaeolithic deposits at El Mnasra and El Harhoura 2, Morocco: implications for Late Pleistocene human–environment interactions along the Atlantic coast of northwest Africa. *J. Hum. Evol.* **62**, 377–394 (2012).
42. Scerri, E. M. L. et al. Did our species evolve in subdivided populations across Africa, and why does it matter? *Trends Ecol. Evol.* **33**, 582–594 (2018).

43. Powell, A., Shennan, S. & Thomas, M. G. Late Pleistocene demography and the appearance of modern human behavior. *Science* **324**, 1298–1301 (2009).
44. Skoglund, P. et al. Reconstructing prehistoric African population structure. *Cell* **171**, 59–71 (2017).
45. Lipson, M. et al. Ancient West African foragers in the context of African population history. *Nature* **577**, 665–670 (2020).
46. Poznik, G. D. et al. Punctuated bursts in human male demography inferred from 1,244 worldwide Y-chromosome sequences. *Nat. Genet.* **48**, 593–599 (2016).
47. Grove, M. Population density, mobility, and cultural transmission. *J. Archaeol. Sci.* **74**, 75–84 (2016).
48. Brooks, A. S. et al. Long-distance stone transport and pigment use in the earliest Middle Stone Age. *Science* **360**, 90–94 (2018).
49. Zeller, E. & Timmermann, A. The evolving three-dimensional landscape of human adaptation. *Sci. Adv.* **10**, eadq3613 (2024).
50. Roberts, P. & Stewart, B. A. Defining the ‘generalist specialist’ niche for Pleistocene *Homo sapiens*. *Nat. Hum. Behav.* **2**, 542–550 (2018).
51. Houlahan, J. E., McKinney, S. T., Anderson, T. M. & McGill, B. J. The priority of prediction in ecological understanding. *Oikos* **126**, 1–7 (2017).
52. Faith, J. T. et al. Rethinking the ecological drivers of hominin evolution. *Trends Ecol. Evol.* **36**, 797–807 (2021).
53. Fretwell, S. D. & Lucas, H. L. On territorial behavior and other factors influencing habitat distribution in birds. I. Theoretical development. *Acta Biotheor.* **19**, 16–36 (1969).
54. Stephen Cantrell, R., Cosner, C., Deangelis, D. L. & Padron, V. The ideal free distribution as an evolutionarily stable strategy. *J. Biol. Dyn.* **1**, 249–271 (2007).
55. Avgar, T., Betini, G. S. & Fryxell, J. M. Habitat selection patterns are density dependent under the ideal free distribution. *J. Anim. Ecol.* **89**, 2777–2787 (2020).
56. Hutchinson, G. E. Concluding remarks. *Cold Spring Harbor Symp. Quant. Biol.* **22**, 415–427 (1957).
57. Banks, W. E. et al. Eco-cultural niche modeling: new tools for reconstructing the geography and ecology of past human populations. *PaleoAnthropology* **2006**, 68–83 (2006).
58. Banks, W. E. et al. Human ecological niches and ranges during the LGM in Europe derived from an application of eco-cultural niche modeling. *J. Archaeol. Sci.* **35**, 481–491 (2008).
59. Timmermann, A. et al. Climate effects on archaic human habitats and species successions. *Nature* **604**, 495–501 (2022).
60. Raia, P. et al. Past extinctions of *Homo* species coincided with increased vulnerability to climatic change. *One Earth* **3**, 480–490 (2020).
61. Elith, J. & Leathwick, J. R. Species distribution models: ecological explanation and prediction across space and time. *Annu. Rev. Ecol. Evol. Syst.* **40**, 677–697 (2009).
62. Beyer, R. M., Krapp, M. & Manica, A. High-resolution terrestrial climate, bioclimate and vegetation for the last 120,000 years. *Sci. Data* **7**, 236 (2020).
63. Yun, K. S. et al. A transient coupled general circulation model (CGCM) simulation of the past 3 million years. *Clim. Past* **19**, 1951–1974 (2023).
64. Zeller, E. et al. Human adaptation to diverse biomes over the past 3 million years. *Science* **380**, 604–608 (2023).
65. Leonardi, M., Boschin, F., Boscato, P. & Manica, A. Following the niche: the differential impact of the last glacial maximum on four European ungulates. *Commun. Biol.* **5**, 1038 (2022).
66. Araújo, M. B. & New, M. Ensemble forecasting of species distributions. *Trends Ecol. Evol.* **22**, 42–47 (2007).
67. Hirzel, A. H., Le Lay, G., Helfer, V., Randin, C. & Guisan, A. Evaluating the ability of habitat suitability models to predict species presences. *Ecol. Model.* **199**, 142–152 (2006).
68. Humphrey, L., Bello, S. M., Turner, E., Bouzouggar, A. & Barton, N. Iberomaurusian funerary behaviour: evidence from Grotte des Pigeons, Taforalt, Morocco. *J. Hum. Evol.* **62**, 261–273 (2012).
69. Stewart, B. A. et al. Ostrich eggshell bead strontium isotopes reveal persistent macroscale social networking across late Quaternary southern Africa. *Proc. Natl Acad. Sci.* **117**, 6453–6462 (2020).
70. Crevecoeur, I., Dias-Meirinho, M.-H., Zazzo, A., Antoine, D. & Bon, F. New insights on interpersonal violence in the Late Pleistocene based on the Nile valley cemetery of Jebel Sahaba. *Sci. Rep.* **11**, 9991 (2021).
71. Thompson, J. C. et al. Early human impacts and ecosystem reorganization in southern-central Africa. *Sci. Adv.* **7**, eabf9776 (2021).
72. Texier, P.-J. et al. A Howiesons Poort tradition of engraving ostrich eggshell containers dated to 60,000 years ago at Diepkloof Rock Shelter, South Africa. *Proc. Natl Acad. Sci.* **107**, 6180–6185 (2010).
73. Texier, P.-J. et al. The context, form and significance of the MSA engraved ostrich eggshell collection from Diepkloof Rock Shelter, Western Cape, South Africa. *J. Archaeol. Sci.* **40**, 3412–3431 (2013).
74. Clark, J. L. & Kandel, A. W. The evolutionary implications of variation in human hunting strategies and diet breadth during the Middle Stone Age of Southern Africa. *Curr. Anthropol.* **54**, S269–S287 (2013).
75. Smith, M. *The Archaeology of Australia's Deserts* (Cambridge Univ. Press, 2013).
76. Böhm, E. et al. Strong and deep Atlantic meridional overturning circulation during the last glacial cycle. *Nature* **517**, 73–76 (2015).
77. Schaebitz, F. et al. Hydroclimate changes in eastern Africa over the past 200,000 years may have influenced early human dispersal. *Commun. Earth Environ.* **2**, 123 (2021).
78. Nutz, A. et al. A 60–50 ka African Humid Period modulated by stadial Heinrich events HE6 and HE5a in northwestern Africa. *Palaeogeogr. Palaeoclimatol. Palaeoecol.* **635**, 111952 (2024).
79. Armstrong, E., Hopcroft, P. O. & Valdes, P. J. A simulated Northern Hemisphere terrestrial climate dataset for the past 60,000 years. *Sci. Data* **6**, 265 (2019).
80. Tierney, J. E., deMenocal, P. B. & Zander, P. D. A climatic context for the out-of-Africa migration. *Geology* **45**, 1023–1026 (2017).
81. Beyer, R. M., Krapp, M., Eriksson, A. & Manica, A. Climatic windows for human migration out of Africa in the past 300,000 years. *Nat. Commun.* **12**, 4889 (2021).

Publisher's note Springer Nature remains neutral with regard to jurisdictional claims in published maps and institutional affiliations.



Open Access This article is licensed under a Creative Commons Attribution 4.0 International License, which permits use, sharing, adaptation, distribution and reproduction in any medium or format, as long as you give appropriate credit to the original author(s) and the source, provide a link to the Creative Commons licence, and indicate if changes were made. The images or other third party material in this article are included in the article's Creative Commons licence, unless indicated otherwise in a credit line to the material. If material is not included in the article's Creative Commons licence and your intended use is not permitted by statutory regulation or exceeds the permitted use, you will need to obtain permission directly from the copyright holder. To view a copy of this licence, visit <http://creativecommons.org/licenses/by/4.0/>.

© The Author(s) 2025

African Pleistocene archaeological deposits included in models (script 1)

Coordinates of archaeological sites are essential for SDMs, as these models are built on the accurate input of spatial occurrence/presence data. Chronometrically dated archaeological layers are also necessary for linking occurrences to the appropriate local climate simulations used in SDMs. Radiometric dating methods provide age estimations before present that are measured on the basis of physical and chemical changes that occur over time⁸². Radiocarbon (¹⁴C), uranium–thorium (U–Th or U-series), optically stimulated luminescence, thermoluminescence and electron spin resonance—among others—are dating methods that provide age estimates in calendar years before present⁸³. In cases in which the age of an archaeological layer was estimated only by non-radiometric methods, it was excluded from subsequent analyses. Non-radiometric dating methods include biochronology, typology and palaeomagnetism. If an archaeological layer was not dated, it was likewise excluded from subsequent analyses. Following the removal of archaeological layers that were not subjected to radiometric dating techniques, further limits were placed on archaeological occurrences included in distribution models and niche area calculations. Any occurrence was excluded if the minimum age subtracted from the maximum age was greater than 20,000 years. These efforts resulted in a database (Supplementary Table 1) with archaeological layers that have: (1) published coordinates; (2) radiometric dates; (3) an age error range less than or equal to 20,000 years; and (4) mean age $\leq 120,000$ and $\geq 14,000$ years. Archaeological sites and layers were compiled from peer-reviewed journals and books published before 5 May 2021. The Role of Culture in Early Expansions of Humans (ROCEEH) has been integrating archaeological, palaeoanthropological, palaeontological and palaeobotanical information into the ROCEEH Out of Africa Database (ROAD) since 2009 (ref. 84). As of May 2021, the team has compiled information on more than 2,000 localities and more than 12,000 assemblages in Africa and Eurasia dated between three million and 20,000 years before present. The information in ROAD is structured into localities (sites) with dated layers that contain assemblages of finds, including artefacts, human fossils, palaeofauna and plant remains, and bibliographic sources. For this study, A.W.K. and M.W. queried ROAD to create a list of archaeological localities in Africa dating between about 500,000 and 10,000 years and reviewed the output for accuracy. The output also included the ages of the layers, as well as radiometric dating results.

Calibration of ¹⁴C radiocarbon ages (script 2)

In our database of archaeological sites, all radiocarbon dates were entered as uncalibrated ages, with the exception of Haua Fteah, for which modelled and calibrated ¹⁴C radiocarbon and optically stimulated luminescence/electron spin resonance ages were entered from Douka et al.⁸⁵. If a single archaeological layer was dated with both ¹⁴C and further chronometric dating methods, the uncalibrated radiocarbon ages were entered in a separate column from the extra radiometric dating methods. For all uncalibrated ¹⁴C ages entered in our database, a basic IntCal20 (ref. 86) calibration for Northern Hemisphere archaeological localities and a basic SHCal20 calibration for Southern Hemisphere archaeological localities was completed using the rcarbon R package⁸⁷. The calibrated ¹⁴C ages were then used to determine the mean age and age error ranges were calculated to the level of 1 σ . If an archaeological layer was dated with ¹⁴C and further methods, our calibrated ¹⁴C mean age and 1 σ error were then combined with the mean age and error range of the other methods to find the mean age used in our models. Note that we did not calibrate ¹⁴C ages using marine calibration curves (Marine20 (ref. 88)), nor did we calculate ΔR values for marine carbonates (but see Reimer and Reimer⁸⁹ for calculation of ΔR for paired marine and terrestrial dates). Marine calibration curves and ΔR values were not

included in our ¹⁴C calibration for two reasons: (1) for many ¹⁴C ages, it is unknown whether dated samples are marine or terrestrial shell and (2) ΔR values are determined regionally based on the nearest samples in the ΔR database but, for much of Africa, the sampling coverage is low. We also did not subtract 180 years before calibration from ¹⁴C ages obtained from ostrich eggshell⁹⁰ (as 180 years is too short a time span to change our models that run in 1,000-year or 2,000-year intervals), nor did we set the northernmost limit for Southern Hemisphere calibration at the Intertropical Convergence Zone, as this boundary is recommended only when seasonal variations are known⁹¹. Instead, we set the boundary between Northern Hemisphere and Southern Hemisphere calibration at the equator, as seasonal variations are unknown for most of the archaeological sites included in the present study. Extended Data Fig. 5 shows the differences between the calibration applied in the present study, opposite hemisphere calibration that was not applied and marine calibration that was not applied. In all cases, the possible dates based on different approaches to calibration fall within a relatively narrow range that would lead, at most, to moving a site to the adjacent 2-ka time window and would have a minimal effect on the local climate assigned to that occurrence. Supplementary Table 2 shows the number assigned to each archaeological site name and layer for Extended Data Fig. 5, as well as uncalibrated ages and errors, calibrated ages and 1 σ errors that were used in the present study and calibrated ages and 1 σ errors that were not used in the present study.

Subdividing MISs

To better visualize how the patterns change through time, and better compare different periods, in our figures, we subdivided MIS stages 4, 3 and 2 to create roughly equal time periods. We subdivided MIS stages 5, 4, 3 and 2 following $\delta^{18}O$ peaks and lows from Cohen and Gibbard⁹². We subdivided MIS 5 into MIS 5e (120–116 ka), MIS 5d (116–104 ka), MIS 5c (104–94 ka), MIS 5b (94–85 ka) and MIS 5a (84–71 ka); MIS 4 was subdivided into early (71–64 ka) and late (64–57 ka); MIS 3 was subdivided into early (57–47 ka), middle (47–39 ka) and late (39–29 ka); and MIS 2 was subdivided into early (29–23 ka) and late (23–15 ka).

Water hosing and Heinrich events

The palaeoclimatic reconstructions from Beyer et al.⁶² do not include water hosing to simulate Heinrich events. To include them, we considered simulations from Armstrong et al.⁷⁹ (although the reference cited focuses on the Northern Hemisphere, the associated simulations of the global circulation model are available on BRIDGE⁹³). In those simulations, Dansgaard–Oeschger and Heinrich events are imposed as a spatial fingerprint with time-varying amplitude to match temperature reconstruction from Greenland ice cores. The spatial fingerprint itself was derived from a freshwater hosing simulation during the Last Glacial Maximum using HadCM3B-M2.1 (ref. 79). As the two runs use slightly different boundary conditions, we computed anomalies for monthly temperature and precipitation between the time slices of interest (that is, with Heinrich events simulated by water hosing) and the simulations for the present, and then added those anomalies to the simulations from the present used by Beyer et al.⁶², working at the original coarse resolution of HadCM3. We then bias-corrected and downscaled those time slices using the same approach as Beyer et al.⁶², thus creating a coherent dataset, and recomputed BIOCLIM variables and ran the BIOME4 global vegetation model, modified to include water hosing and Heinrich events. At the end, we had 17 BIOCLIM variables available (BIO 2 and BIO 3 could not be computed as they are based on daily rather than monthly summaries) and two vegetation variables (net primary productivity and LAI).

SDM methods (scripts s01 to s16)

Variable selection. Variable selection was performed using the R package tidysdm⁹⁴. The palaeoclimatic reconstructions (Beyer et al.⁶² with added Heinrich events; see section above) were stored as a netCDF file

and were accessed using the R package `pastclim`⁹⁵ (dataset = “custom”). We defined which variables to use for our analyses using the equivalent of the `plot_pres_vs_bg()` and `dist_pres_vs_bg()` functions in `tidysdm`⁹⁴. We used an older version of the function `tidysdm::plot_pres_vs_bg()` to create a violin plot comparing the distribution over the variable space of the occurrences versus a representative sample of the background. The latter was obtained by randomly drawing 10,000 points from each time slice over the whole area and period considered (Extended Data Fig. 6a). The variables for which humans seemed to occupy the climatic space differently from what was available in the environment suggest non-random use of the variable itself, supporting the idea that they would be more meaningful to reconstruct the distribution of the species (see, for reference, the function `tidysdm::dist_pres_vs_bg()`). Finally, among these informative variables, we extracted a set of variables that showed a correlation among each other below a threshold of 0.8 (Extended Data Fig. 6b), leaving: LAI, temperature annual range (BIO 7), mean temperature of the wettest quarter (BIO 8), mean temperature of the warmest quarter (BIO 10) and precipitation of the wettest quarter (BIO 16).

Chronological uncertainty and temporal sampling bias. Each radiometric date is associated with a specific chronological uncertainty, expressed as a range (most likely date and plus/minus). To take into account such uncertainty, we performed our analyses as follows. We created 100 independent datasets: for each of them, the spatial coordinates of all occurrences (= radiometrically dated archaeological layer) were associated to an age that was resampled from the whole chronological range of the date. Such sampling was performed following a truncated normal distribution identified by the mean and the plus/minus as 2σ (ref. 96).

When looking at the number of our occurrences through time (as exemplified by their mean age shown in Extended Data Fig. 1a), there is a marked increase in the number of layers observed through time. This pattern is most likely the result of a combination of an increasing number of human occupations through time, a conservation bias (with more recent traces of occupation being more likely to have survived than older ones) and the differential use of the available radiometric dating techniques (for example, ¹⁴C is only available up to around 50 ka). To account for all of these factors, each of the resampled datasets was randomly subsampled to generate a homogeneous distribution in the number of occurrences available through time (thus giving us constant sampling effort through time) using the following procedure. We identified that, at 78 ka, there is a boundary between an older period with a low number of occurrences (on average between zero and eight per time slice, varying on the basis of the chronological resampling) and a more recent period in which there is much more data available. For each resampling, we then subset each time slice from the more recent period to the number of occurrences observed in a randomly sampled older time slice (Extended Data Fig. 1).

To adequately represent the existing climatic space (that is, background) in our SDMs, each of these resulting, constant-effort datasets was coupled with a random sampling, for each observation, of 200 random locations matched by time. This resulted in $n = 100$ datasets (= ‘repeats’) of randomly sampled and dated occurrences and differently sampled background points. We independently repeated our analyses for each of these datasets, thus accounting for the stochasticity of resolving the time uncertainty, the sampling biases and the choice of background points. From this stage, all analyses were repeated independently using two sets of palaeoclimatic simulations: Beyer et al.⁶² with Heinrich events and PCESM^{63,64}.

Modelling. We then used GAMs (`mgcv` package in R (ref. 97)) to fit two possible models: a ‘changing-niche’ model that included interactions of each environmental variable with time (fitted as tensor products) and a ‘fixed-niche’ model that included the environmental variables as

covariates but lacking interactions with time⁶⁵. Thus, for the fixed-niche model, the `mgcv` GAM formula is

```
gam(obs~ti(bio07, k=4) + ti(bio08, k=4) + ti(bio10, k=4) +
    ti(bio16, k=4) + ti(lai, k=4),
    data=data, family='binomial')
```

Here human presence/absence (`obs`) is modelled as the sum of five nonlinear functions (of the four bioclimatic variables and LAI). Each function `ti()` denotes a tensor product smooth term created using thin plate regression splines, in which each spline is composed of $k=4$ basis functions. `family='binomial'` indicates that the response variable (`obs`) follows a binomial distribution and the link function is the logit function. `data` denotes the R data frame containing the response and predictor variables.

For the changing-niche model, we have

```
gam(obs~ti(bio07, k=4) + ti(bio08, k=4) + ti(bio10, k=4) +
    ti(bio16, k=4) + ti(lai, k=4) + ti(time_bp, k=4) +
    ti(time_bp, bio07, k=4) + ti(time_bp, bio08, k=4) +
    ti(time_bp, bio10, k=4) + ti(time_bp, bio16, k=4) +
    ti(time_bp, lai, k=4),
    data=data, family='binomial')
```

This model uses an extra five bivariate functions, each of which includes time before present (`time_bp`) as a second argument, as well as the relevant bioclimatic variable or LAI. Note that both models use bioclimatic and LAI values corresponding to the time and location of the human presence data (`obs`), but only the second model considers nonlinear interactions between the bioclimatic and LAI variables with time, whereas the first model only includes a univariate time function term. For a formal definition of the univariate and bivariate thin plate regression splines, `ti(x)` and `ti(t,x)`, respectively, we refer readers to Wood⁹⁸ (specifically section 2, starting on page 1,026, as well as subsection 2.1 ‘Nesting and ANOVA decomposition’ on page 1,028, which provides a rationale for how the models are compared). A comprehensive description of how GAMs are fitted in `mgcv` is given by Wood⁹⁷.

For all GAMs, we set $k = 4$ as the maximum threshold for the degrees of freedom of the splines; this value provides a reasonable compromise between allowing the relationship to change through time but avoiding excessive overfitting⁹⁹.

Residual checks. For each repeat, we performed standard checks on the residuals of the models using the `DHARMa` package in R (ref. 100), including the following tests: Kolmogorov–Smirnov for correct distribution, dispersion and outliers. Kolmogorov–Smirnov deviation was significant for six repeats in the changing-niche model (numbers 1, 4, 24, 37, 52 and 56) and five repeats for the fixed-niche model (numbers 1, 4, 24, 37 and 56). Outlier test deviation was significant for eight repeats of the changing-niche model (numbers 25, 38, 67, 69, 74, 78, 85 and 95) and 11 for the fixed-niche model (numbers 18, 24, 25, 30, 38, 67, 74, 77, 78, 85 and 95). All other tests and repeats were non-significant. Visual inspection of these deviations revealed that they were mostly capturing patterns of very small magnitude owing to the high power associated with the large size of the datasets (as a result of the large number of background points) and thus were judged not to affect an analysis. A comparison of models with outliers and models without outliers showed that the model effects were qualitatively similar, thus confirming that the outliers were not leading to artefactual conclusions. We also tested for spatial autocorrelation in the residuals calculating Moran’s I (ref. 101) with the same package. Moran’s I values were statistically significant (P -value < 0.05) but negligible (<0.01 on a scale between 0 and 1) in all cases (Supplementary Table 3).

Model evaluation. For each repeat, we compared the fixed-niche and changing-niche models using the AIC and found strong support for the latter in all cases (Extended Data Fig. 7a). We then evaluated the fit of the changing-niche models with the BCI¹⁰², which is specifically designed to be used with presence-only data, setting an acceptance threshold of Pearson's correlation coefficient > 0.7 (ref. 67) (Extended Data Fig. 7b).

Ensemble. To achieve more robust predictions⁶⁶, we calculated the mean and median ensembles across the 100 repeats in the following way. We selected only repeats that had an AIC > 2, hence strongly supporting the changing-niche model (91/100 for Beyer et al.⁶² with Heinrich events, 95/100 for PCESM^{63,64}; Extended Data Fig. 7a). From them, we kept only repeats with a BCI > 0.7 (which accounted for 70% for Beyer et al.⁶² with Heinrich events and 55% for PCESM^{63,64}; Extended Data Fig. 7b). From this selection of repeats, we created four ensembles (two for each palaeoclimatic model) by computing the mean and median of the predictions. Then, to estimate the goodness of fit of each ensemble, we computed the mean and median of the BCI estimated for each of their individual repeats (note that each repeat had a different set of occurrences and background points as a result of the random resampling).

Visualizing potential distribution through time (Fig. 3). As the mean ensemble performed better than the one based on the median, it was used to visualize how the potential distribution of humans changed through time. To incorporate the uncertainty associated with the model, the predicted probabilities of occurrence were transformed into binary (presence or absence) using three different thresholds. The first one (darkest colour in Fig. 3) represents the minimum predicted area encompassing 90% of our occurrences and identifies the 'core area' suitable for humans (that is, the space most likely occupied). We similarly plotted a 'peripheral area' encompassing 95% and the 'total area' encompassing 99% of occurrences. This was done using a modified version of the function `ecospat.mpa()` from the `ecospat` R package¹⁰³, in which no rounding of the digit is performed. To better visualize how the reconstructed potential distribution changed through time, we calculated for each climatic period the mean of the projections from the individual time slides. A similar procedure has been applied to the fixed-niche models, (using only the repeats with AIC < 2), for which the equivalent of Fig. 3 is available as Extended Data Fig. 2).

Visualizing niche changes through time (Extended Data Figs. 3 and 9). To visualize the changing impact of different BIO variables through time in the niche-changing model, we used the function `draw.gam()` from the R package `gratia`¹⁰⁴ following Leonardi et al.⁶⁵. This function plots the interactions between time and each of the BIO variables. The result is a heat map with time represented on the x axis and the values of the variable of interest on the y axis. Within the plot, the surface colour ('partial effect') shows the effect on the probability of occurrence: red means an increased and blue a decreased probability compared with what would be expected on the basis of the mean value of other variables (the black lines are isoclines to aid reading the changes in the surface). We created partial effect surfaces for all repeats included in each ensemble and then plotted the mean surface, which captures consistent signals across all randomized sets of background points (Extended Data Fig. 3 for Beyer et al.⁶² with added Heinrich events and Extended Data Fig. 9 for PCESM^{63,64}).

Analysing the SDM output (script s13). The analyses described in this section were performed on the regions combining the core and peripheral areas (that is, dark and medium purple in Fig. 3; from now on: suitable habitat). For each time slice, we subdivided the suitable habitat into three different classes of biomes (forest, savannah and desert) based on BIOME4 (ref. 62) reconstructions. Ideally, we would have done it for the finer subdivisions provided by the original model,

but the limited number of occurrences in the archaeological record prevents us from performing any formal analysis at this disaggregated level (for example, we only have two points for tropical rainforest). The list of biomes included in each class can be found in Supplementary Table 4. We then aggregated the results by MIS by keeping for each cell the most common biome class within the given period (Fig. 4a).

To visualize how much of the suitable area falls into each biome class (Fig. 4b), we performed the following steps. First, we summarized the five BIO climatic variables by computing the first two principal components, pooling all land cells for all of the time steps (that is, creating a principal component analysis that represents the full climatic space of Africa for the whole period considered in this research). Then, in that 2D space, for each biome class and time step, we calculated the area covered by the 2D kernel that includes 99% of the suitable cells (core and peripheral areas) within that biome class¹⁰⁵. We repeated this procedure separately for the changing-niche and fixed-niche models, which are presented in Extended Data Fig. 4).

Testing against different palaeoenvironmental simulations (script s16). To correct for the potential biases linked to the specific palaeoclimatic simulations used, we repeated the whole set of analyses described (excluding the standard checks on the residuals and the calculation of Moran's *I*) with the PCESM^{63,64} climatic simulations. The AIC and BCI are comparable with the analyses presented here (Extended Data Fig. 7a,b), as are the patterns in the response surfaces of the GAMs, in which we consistently observe a change during MIS 4 (Extended Data Fig. 9). Projections of the fixed-niche and changing-niche models and results of the biome analyses are available as Extended Data Figs. 8b, 4 and 10).

Figure design. The cartographic representation of Africa in Fig. 1 was originally developed on QGIS 3.22 Białowieża with WGS 84 projection. Geolocated archaeological layers were superimposed and colour-coded on the basis of chronology (Fig. 1a). Overlapping sites in Fig. 1a were stacked in ascending chronological order, with older sites overlapping younger sites. A map with archaeological occurrence/layer density per square kilometre (Fig. 1b) was developed using an automated density cluster function on QGIS 3.22 Białowieża. The resulting cartographic representations were exported as .svg format and composed on Adobe Illustrator 2025. Figures 2, 3 and 4 originated as .svg files from R. Cartographic panels were processed in Adobe Photoshop 2023 and subsequently designed and composed using Adobe Illustrator 2023.

Reporting summary

Further information on research design is available in the Nature Portfolio Reporting Summary linked to this article.

Data availability

Climate data extracted from refs. 62–64. Archaeological site data from ref. 84. All archaeological data included in this study are cited and provided in the Supplementary Information. All palaeoclimate data included in this study are cited and provided in the Supplementary Information. Palaeoclimate data are archived and available at <https://figshare.com/s/2c4253ae69d37268a8>.

Code availability

Code to perform all analyses in this study is available at the following links: script 1: <https://figshare.com/s/d7de3f42aa9e2423bfb5>; script 2: <https://figshare.com/s/291f499a2b7907dfb62b>; scripts s01 to s16: <https://figshare.com/s/3570c73e7a1d6a5e783e>.

82. Aitken, M. J. & Stokes, S. in *Chronometric Dating in Archaeology* (eds Taylor, R. E. & Aitken, M. J.) 1–30 (Springer, 1997).

83. Taylor, R. E. & Aitken, M. J. (eds). *Chronometric Dating in Archaeology* (Springer, 1997).

84. Kandel, A. W. et al. The ROCEEH Out of Africa Database (ROAD): a large-scale research database serves as an indispensable tool for human evolutionary studies. *PLoS One* **18**, e0289513 (2023).
85. Douka, K. et al. The chronostratigraphy of the Haua Fteah cave (Cyrenaica, northeast Libya). *J. Hum. Evol.* **66**, 39–63 (2014).
86. Reimer, P. J. et al. The IntCal20 Northern Hemisphere radiocarbon age calibration curve (0–55 cal kBP). *Radiocarbon* **62**, 725–757 (2020).
87. Crema, E. R. & Bevan, A. Inference from large sets of radiocarbon dates: software and methods. *Radiocarbon* **63**, 23–39 (2021).
88. Heaton, T. J. et al. Marine20—the marine radiocarbon age calibration curve (0–55,000 cal BP). *Radiocarbon* **62**, 779–820 (2020).
89. Reimer, R. W. & Reimer, P. J. An online application for ΔR calculation. *Radiocarbon* **59**, 1623–1627 (2017).
90. Vogel, J. C., Visser, E. & Fuls, A. Suitability of ostrich eggshell for radiocarbon dating. *Radiocarbon* **43**, 133–137 (2001).
91. Hogg, A. G. et al. SHCal20 Southern Hemisphere calibration, 0–55,000 years cal BP. *Radiocarbon* **62**, 759–778 (2020).
92. Cohen, K. M. & Gibbard, P. L. Global chronostratigraphical correlation table for the last 2.7 million years, version 2019 Q1–500. *Quat. Int.* **500**, 20–31 (2019).
93. Valdes, P. J. Earth systems modelling within Bridge: a database of model simulations. *BRIDGE* <https://www.paleo.bristol.ac.uk/resources/simulations/> (2022).
94. Leonardi, M., Colucci, M., Pozzi, A. V., Scerri, E. M. L. & Manica, A. *tidysdm*: leveraging the flexibility of *tidymodels* for species distribution modelling in R. *Methods Ecol. Evol.* **15**, 1789–1795 (2024).
95. Leonardi, M., Hallett, E. Y., Beyer, R., Krapp, M. & Manica, A. *pastclim* 1.2: an R package to easily access and use paleoclimatic reconstructions. *Ecography* **2023**, e06481 (2023).
96. Will, M., Krapp, M., Stock, J. T. & Manica, A. Different environmental variables predict body and brain size evolution in *Homo*. *Nat. Commun.* **12**, 4116 (2021).
97. Wood, S. N. *Generalized Additive Models: An Introduction with R, Second Edition* (Chapman and Hall/CRC, 2017).
98. Wood, S. N. Low-rank scale-invariant tensor product smooths for generalized additive mixed models. *Biometrics* **62**, 1025–1036 (2006).
99. Clay, T. A., Phillips, R. A., Manica, A., Jackson, H. A. & de L. Brooke, M. Escaping the oligotrophic gyre? The year-round movements, foraging behaviour and habitat preferences of Murphy's petrels. *Mar. Ecol. Prog. Ser.* **579**, 139–155 (2017).
100. Hartig, F. DHARMa: Residual Diagnostics for Hierarchical (Multi-Level / Mixed) Regression Models. R package version 0.4.4. <https://CRAN.R-project.org/package=DHARMa> (2021).
101. Moran, P. A. P. Notes on continuous stochastic phenomena. *Biometrika* **37**, 17–23 (1950).
102. Boyce, M. S., Vernier, P. R., Nielsen, S. E. & Schmiegelow, F. K. A. Evaluating resource selection functions. *Ecol. Model.* **157**, 281–300 (2002).
103. Di Cola, V. et al. *ecospat*: an R package to support spatial analyses and modeling of species niches and distributions. *Ecography* **40**, 774–787 (2017).
104. Simpson, G. L. *gratia*: Graceful 'ggplot'-Based Graphics and Other Functions for GAMs Fitted Using 'mgcv'. R package version 0.6.0. <https://CRAN.R-project.org/package=gratia> (2021).
105. Broennimann, O. et al. Measuring ecological niche overlap from occurrence and spatial environmental data. *Global Ecol. Biogeogr.* **21**, 481–497 (2012).

Acknowledgements This project was financed by the Max Planck Society. M.L., R.B., M.K. and A.M. were financed by the ERC Consolidator Grant 647787 'LocalAdaptation'. M.L. and A.M. were financed by the Leverhulme Research Grant RPG-2020-317. A.W.K. is financed by the Heidelberg Academy of Sciences and Humanities, which is promoted by the Joint Science Conference of the Federal and State governments of the Republic of Germany within the framework of the Academies' Programme. Funding comes from the Federal Ministry of Education, Science and Research and the state of Baden-Württemberg's Ministry of Science, Research and the Arts.

Author contributions E.Y.H., M.L., A.M. and E.M.L.S. conceived the study. J.N.C. collected data for West African archaeological sites and produced the figures and illustrations in this manuscript. M.W. and A.W.K. queried ROAD to create a list of archaeological localities in Africa dating between 500,000 and 10,000 years and reviewed the output for accuracy. The output also included the ages of the layers as well as radiometric dating results for calibration. E.Y.H. filtered archaeological localities used in this study and calibrated radiocarbon ages. M.W., A.W.K. and E.Y.H. reviewed archaeological localities and ages as well as those from ROAD for accuracy. R.B., M.K. and A.M. provided palaeoclimate data. M.L. and A.M. developed the time-varying niche modelling methods. M.L. performed the SDM analyses. M.L., A.M. and E.Y.H. analysed the SDM output. A.M. supervised the formal analysis, methodology, software and validation. E.Y.H., M.L., A.M. and E.M.L.S. wrote the original drafts of this manuscript. All authors commented on and edited the final version of the manuscript.

Funding Open access funding provided by Max Planck Society.

Competing interests The authors declare no competing interests.

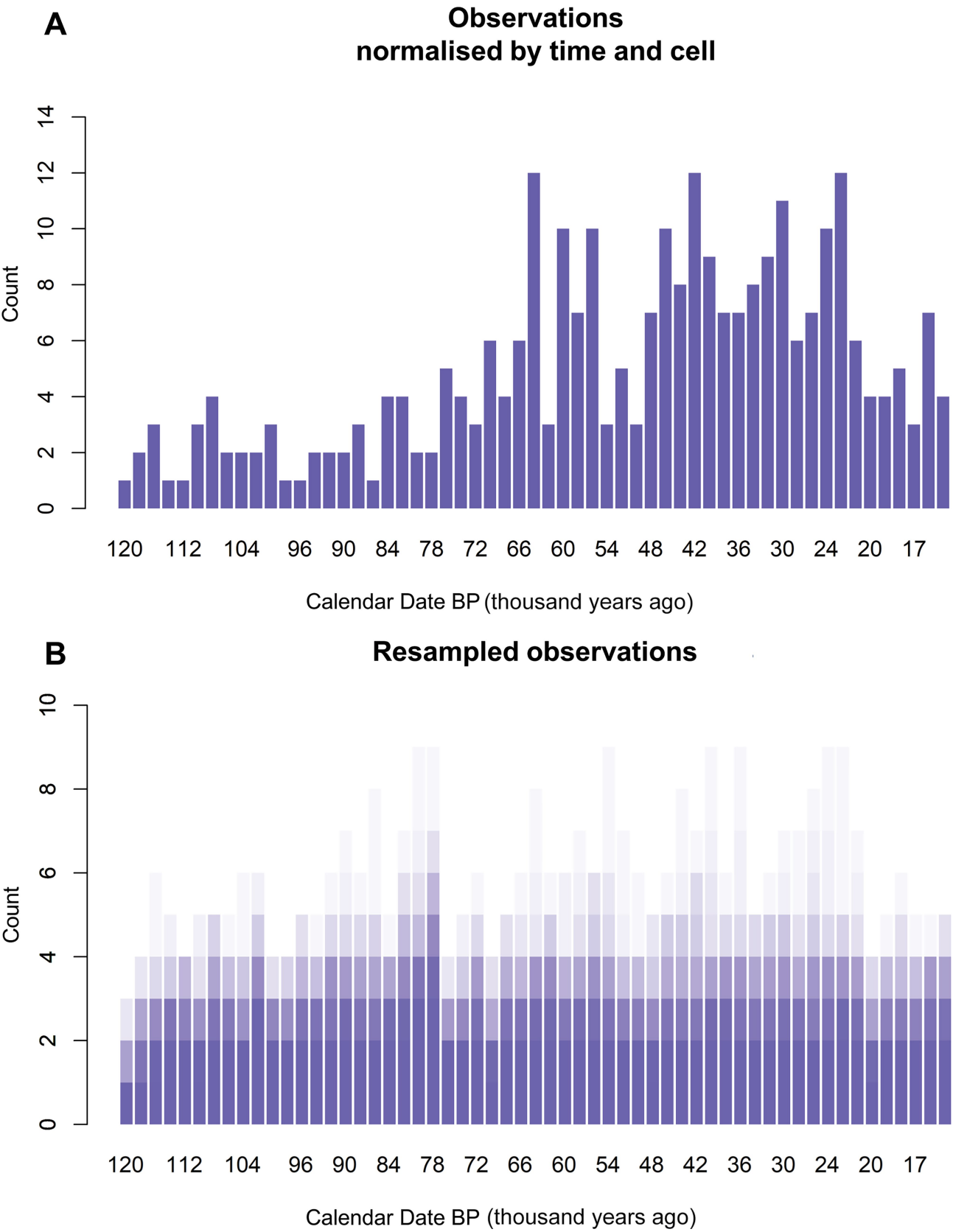
Additional information

Supplementary information The online version contains supplementary material available at <https://doi.org/10.1038/s41586-025-09154-0>.

Correspondence and requests for materials should be addressed to Emily Y. Hallett, Michela Leonardi, Andrea Manica or Eleanor M. L. Scerri.

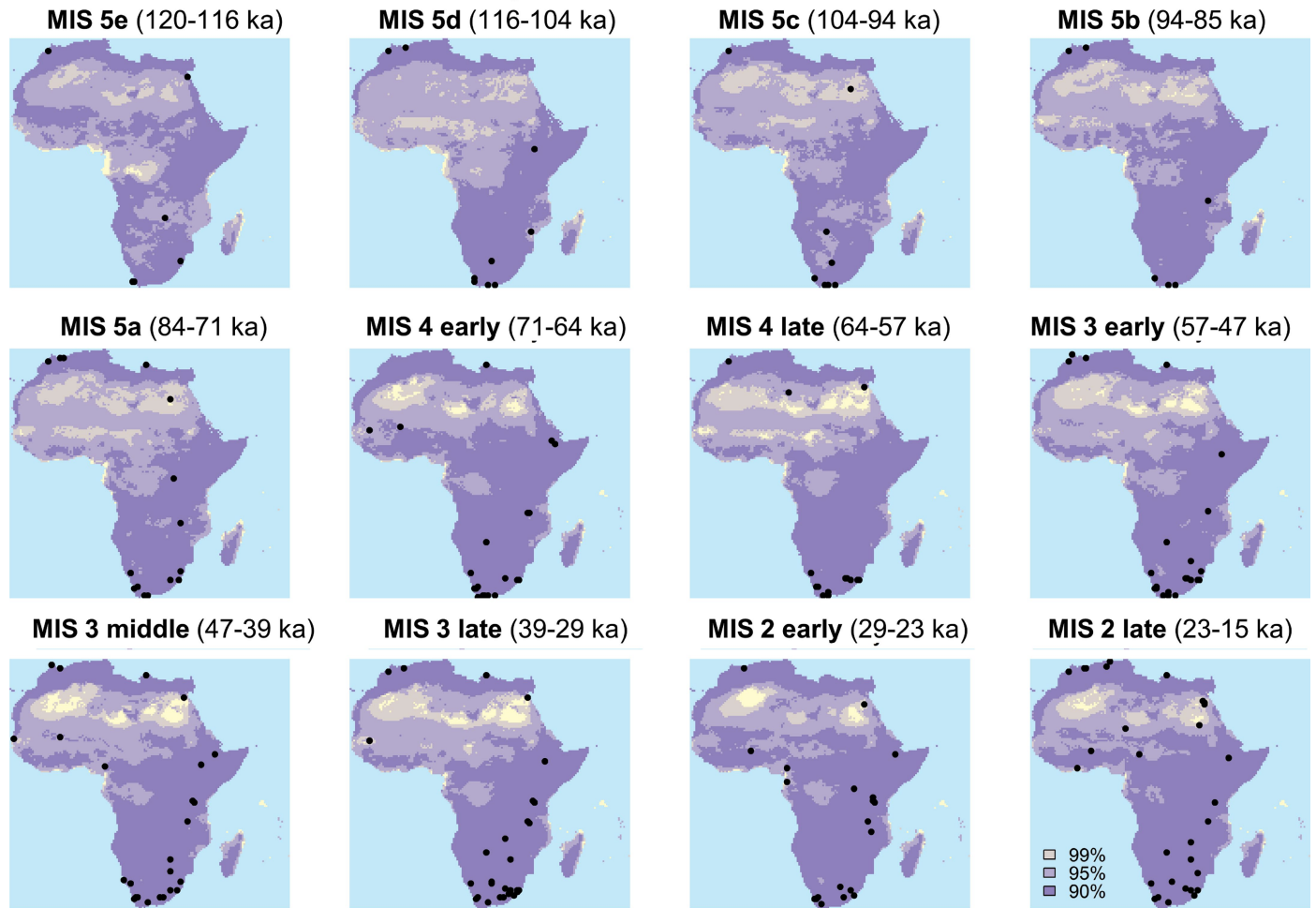
Peer review information *Nature* thanks Francesco d'Errico, Jayne Wilkins, William Banks, Axel Timmermann and the other, anonymous, reviewer(s) for their contribution to the peer review of this work.

Reprints and permissions information is available at <http://www.nature.com/reprints>.



Extended Data Fig. 1 | Histogram of archaeological occurrences and resampled occurrences through time. a, Histogram of archaeological occurrences (in ka), using the mean age of each layer. **b**, Histogram of resampled occurrences through time (in ka) (100 resamples per layer).

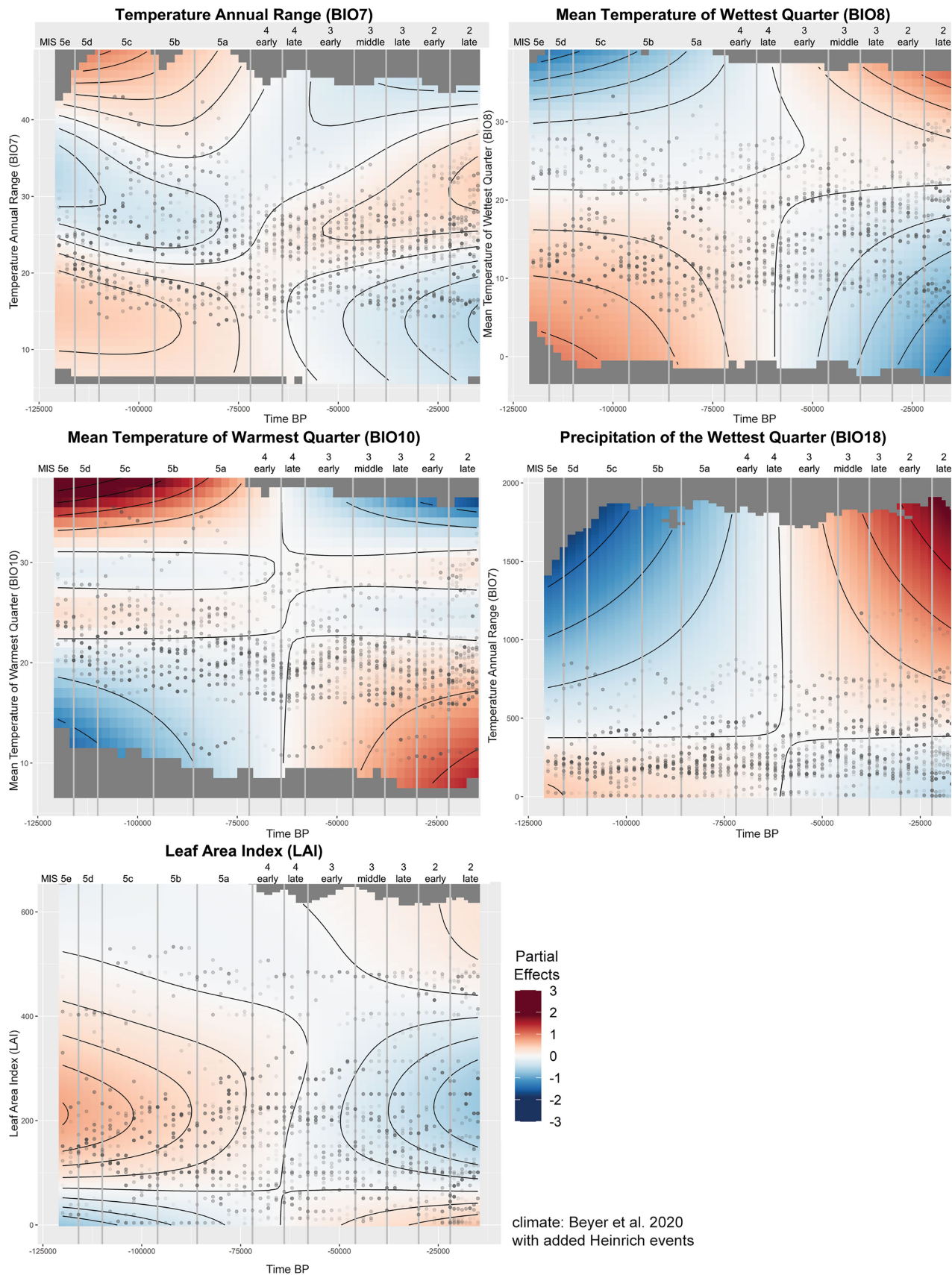
Projection fixed-niche model



climate: Beyer et al. 2020 with added Heinrich events

Extended Data Fig. 2 | Projection of the fixed-niche model through time (using climate reconstructions from Beyer et al.⁵⁷ with added Heinrich events). The core (90% of occurrences), peripheral (95% of occurrences) and total area (99% occurrences) are shown.

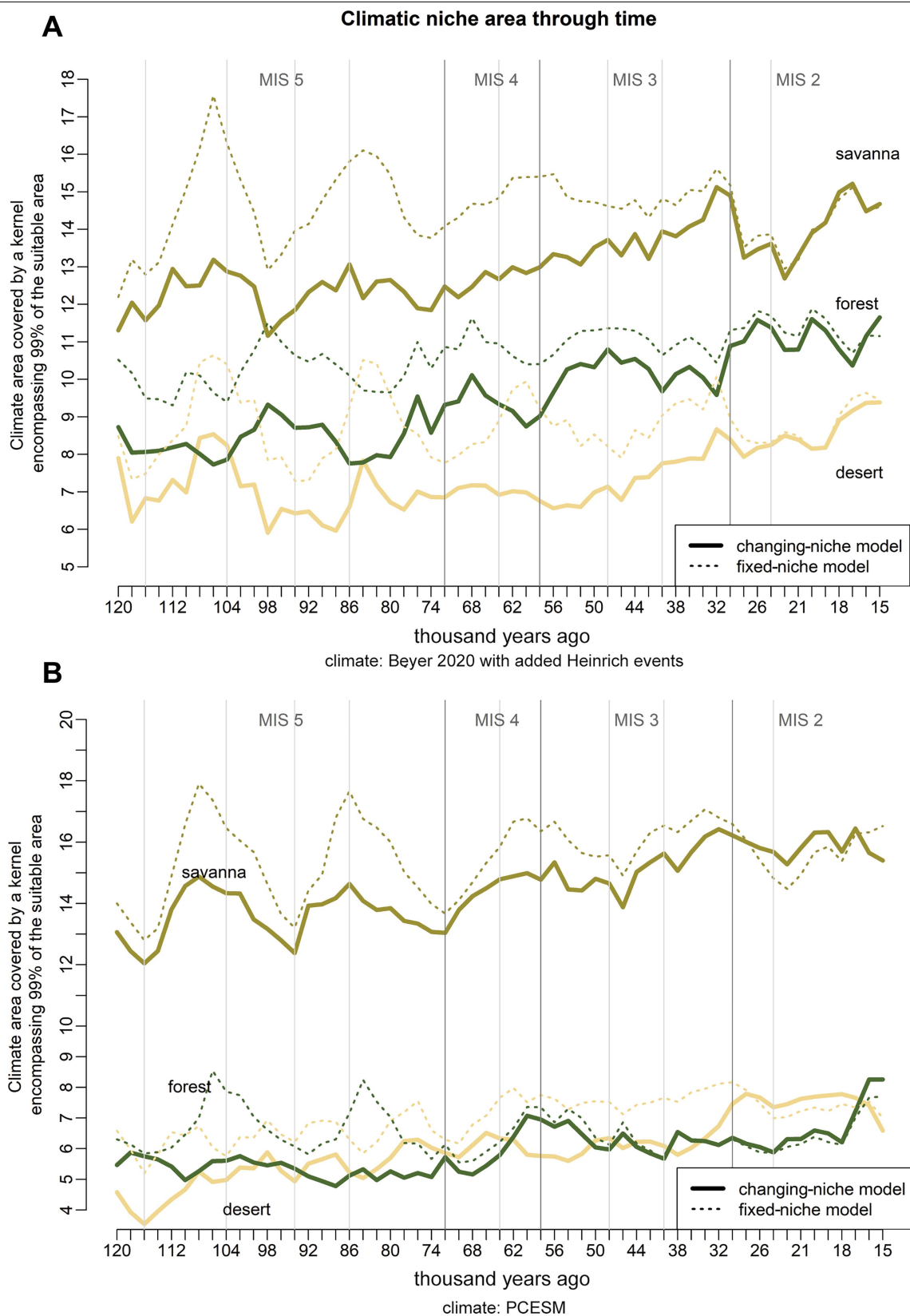
Interaction with time in the models



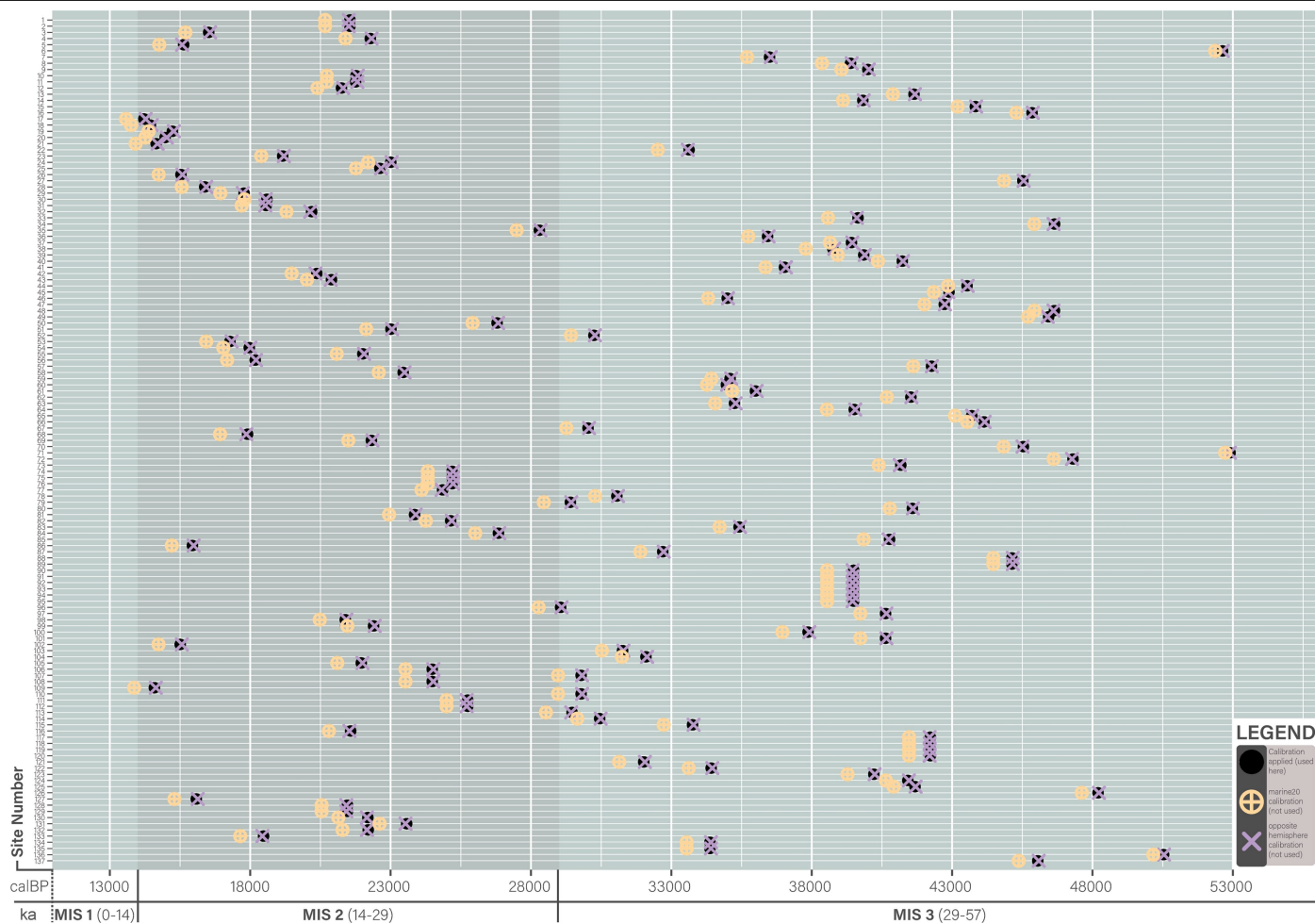
Extended Data Fig. 3 | See next page for caption.

Extended Data Fig. 3 | Interaction with time in the models built using the Beyer et al.⁵⁷ climatic reconstructions with added Heinrich events.
Homo sapiens resampled occurrences are shown as grey dots (overlapping points are shown in darker shades based on their number). The partial effects of the GAMs (z axis, colour shading) show the interaction between the variable of interest (y axis) and time (x axis). Here we present the mean values of the

partial effects plots over 100 repeats. The red shading represents favourable variable space (used more than expected by chance given the availability in the whole continent) and blue represents less favourable variable space. The y variables used in the GAMs are: temperature annual range (BIO 7), mean temperature of the wettest quarter (BIO 8), mean temperature of the warmest quarter (BIO 10), precipitation of the wettest quarter (BIO 16) and LAI.

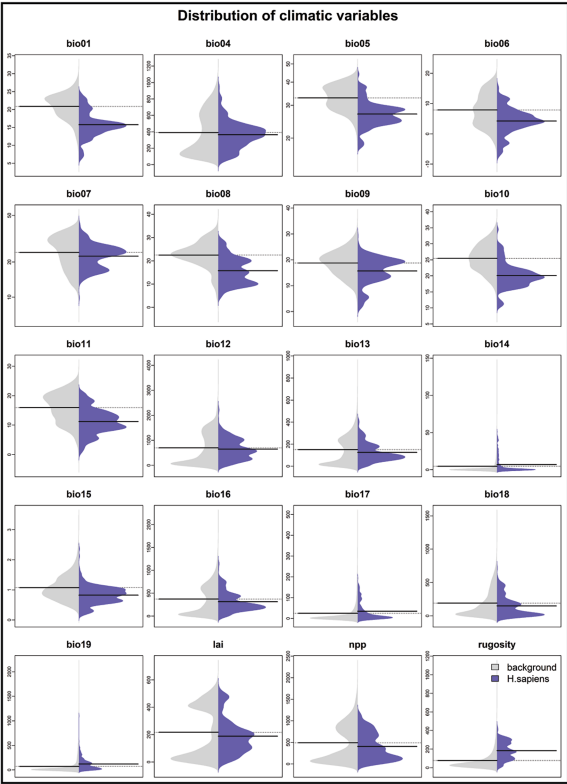


Extended Data Fig. 4 | Comparison of the niche area. Encompassing 95% of presences covered through time for each of the main biomes in the changing-niche model (solid lines) and the fixed-niche model (dashed lines). **a**, Beyer et al.⁵⁷ modified to include Heinrich events. **b**, PCESM^{58,59}.

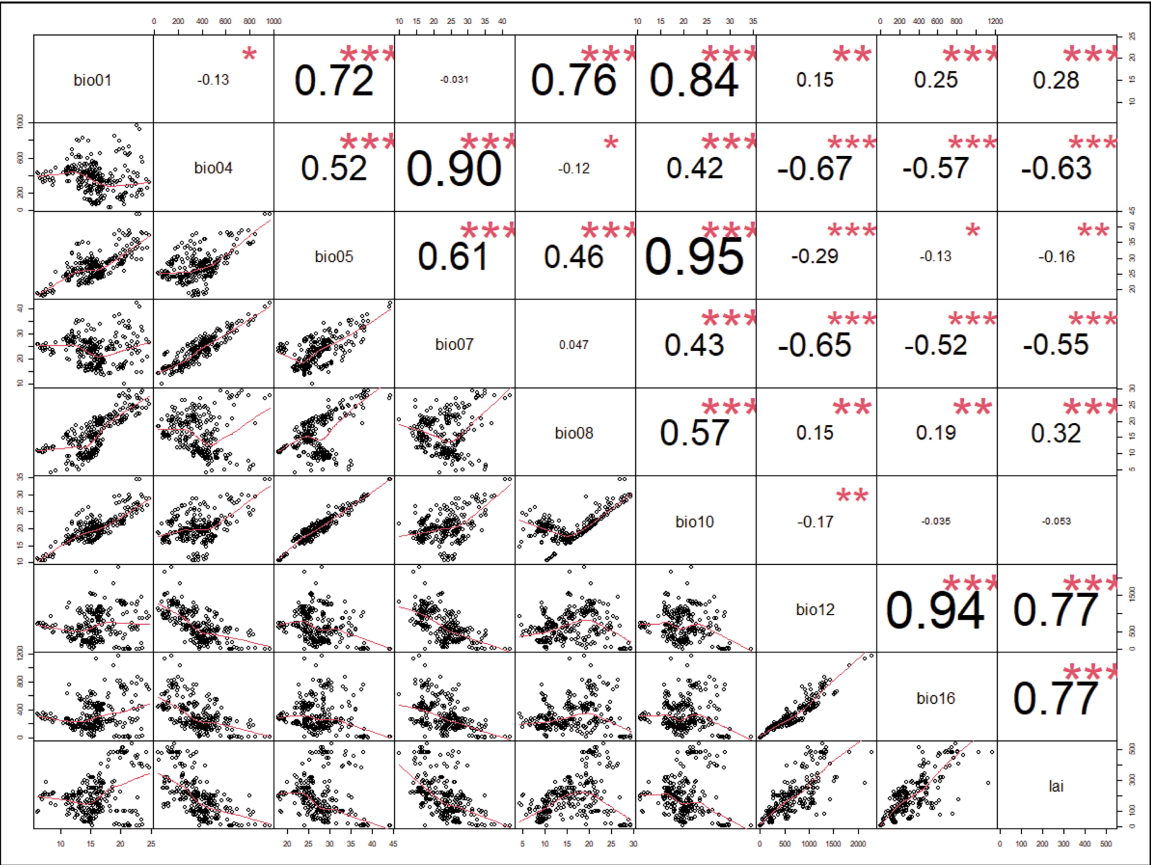


Extended Data Fig. 5 | Calibration plots. The differences between the calibration applied in the present study (black), opposite hemisphere calibration that was not applied (purple) and marine calibration (orange) that was not applied.

A



B



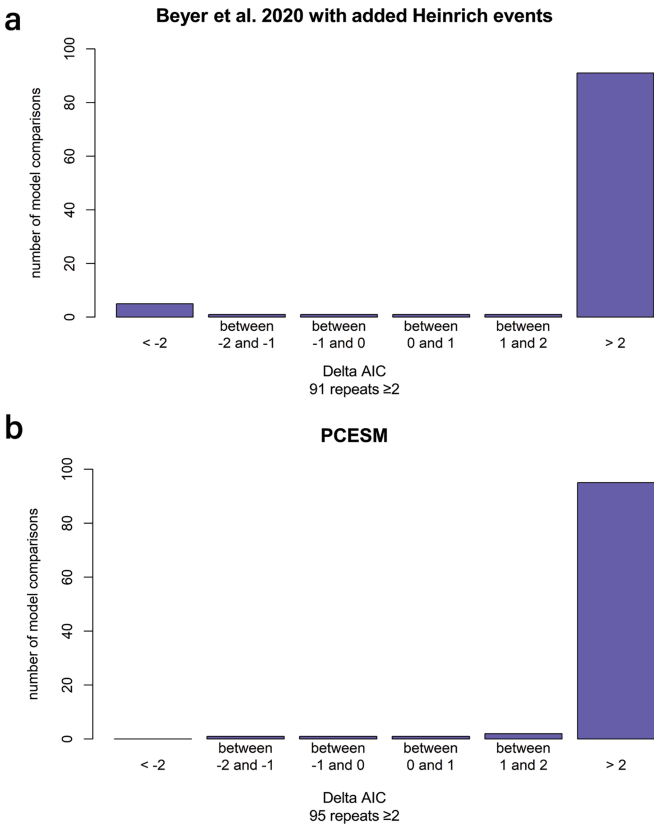
Extended Data Fig. 6 | See next page for caption.

Extended Data Fig. 6 | Distribution and cross-correlation of climatic variables. **a**, Distribution of climatic variables in the archaeological occurrences through time versus the whole continent (background). Climate: Beyer et al.⁵⁷ with added Heinrich events. **b**, Cross-correlation of climatic variables (dataset: Beyer et al.⁵⁷ with added Heinrich events) for *H. sapiens* occurrences.

The lower-left triangle shows the scatter plot between pairs of variables. The upper-right triangle contains the numerical values of the cross-correlations, with bigger sizes corresponding to larger distance from 0. The asterisks in each cell represent the level of significance of the corresponding value.

A

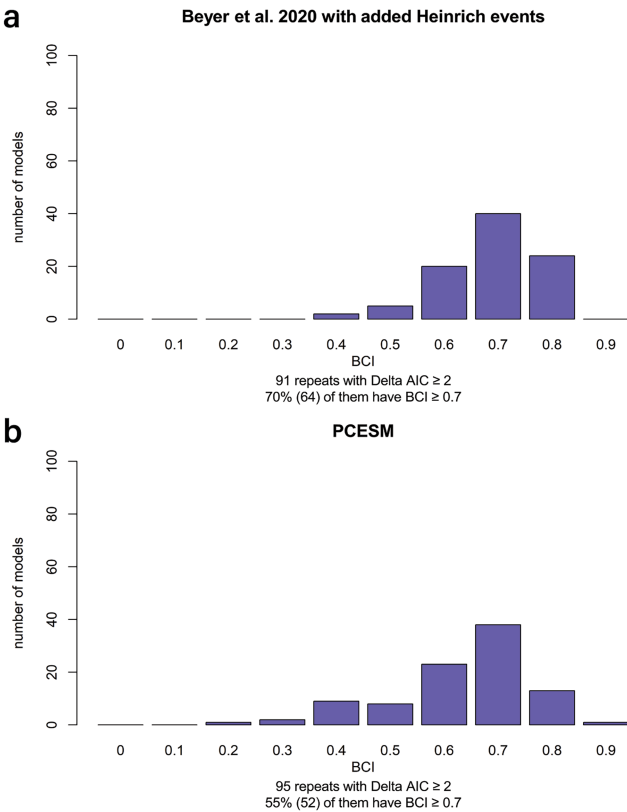
Delta AIC (fixed-niche - changing niche model)



Extended Data Fig. 7 | Histogram of delta AIC and BCI.
A, Histogram of delta AIC between the fixed-niche versus changing-niche model in the 100 repeats. A score ≥ 2 supports the time-varying-niche model. **a**, Beyer et al.⁵⁷ with added Heinrich events, 91 repeats have a delta AIC ≥ 2 . **b**, PCESM^{58,59}, 95 repeats have a delta AIC ≥ 2 . **B**, BCI for the changing-niche model. The BCI has only been calculated on the repeats having an AIC ≥ 2 , hence supporting the changing-niche model. These have been used to build the ensembles. **a**, Beyer et al.⁵⁷ with added Heinrich events, 91 repeats with AIC ≥ 2 ; among them, 70% (64) have BCI ≥ 0.7 . **b**, PCESM^{58,59}, 95 repeats with AIC ≥ 2 ; among them, 55% (52) have BCI ≥ 0.7 .

B

Boyce Continuous Index (changing niche model with AIC ≥ 2)



A

Comparison of climatic reconstructions

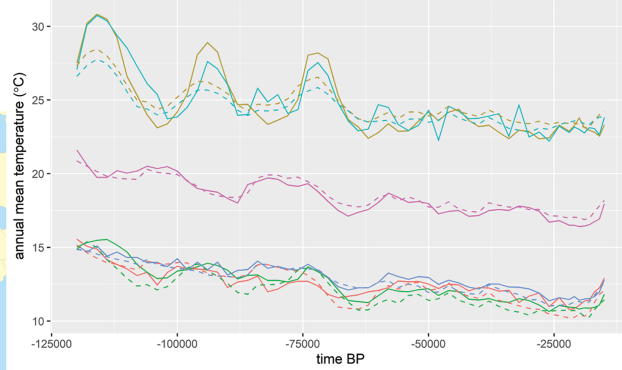
Locations



Legend

- Beyer et al. 2020 with added Heinrich events
- - - PCESM

Annual mean temperature (BIO1)

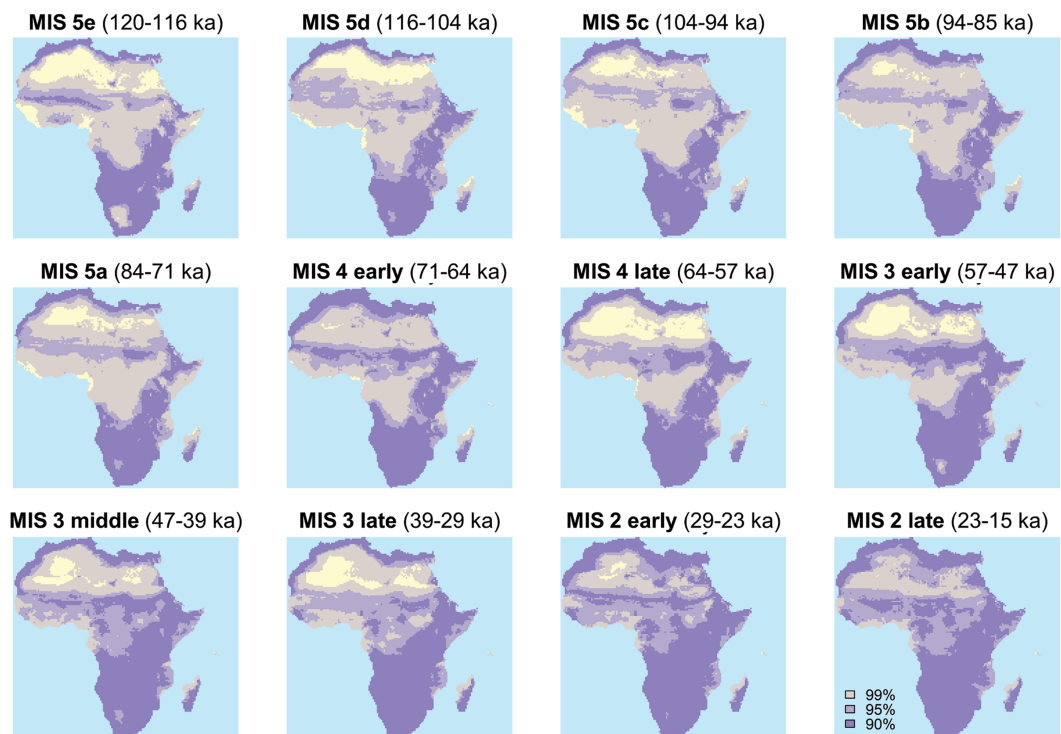


Annual precipitation (BIO12)



B

Projection changing-niche model, PCESM



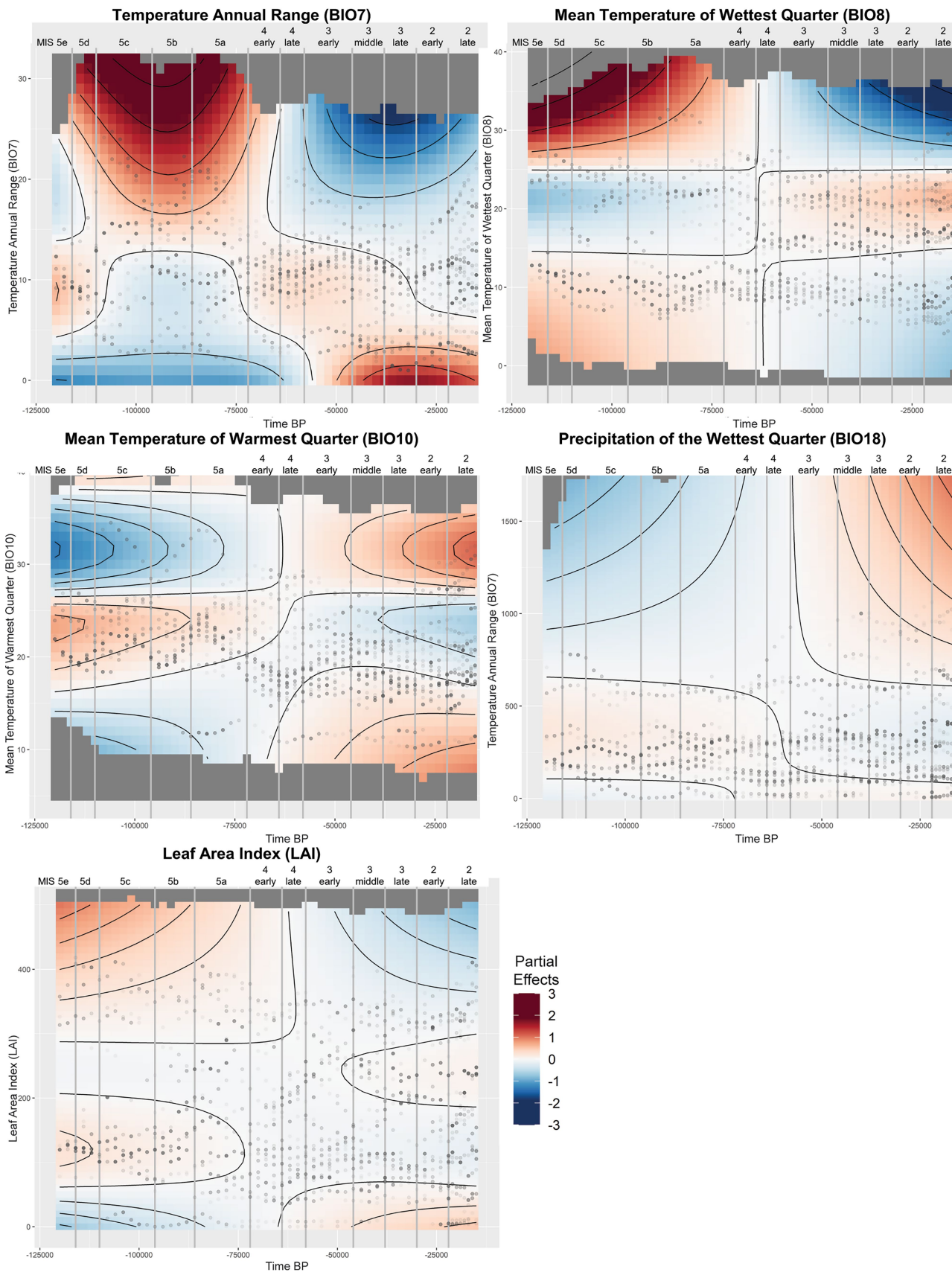
Extended Data Fig. 8 | Comparison of climate simulations and projection of the changing niche through time using PCESM^{58,59} climate simulations.

a. Comparison of the Beyer et al.⁵⁷ with added Heinrich events (continuous lines) and PCESM^{58,59} (dashed lines) simulations. Mean annual temperature (BIO 1)

and total annual precipitation (BIO 12) for six African locations are shown.

b. Projection of the changing-niche model through time (using climate simulations from PCESM^{58,59}). The core (90% of occurrences), peripheral (95% of occurrences) and total area (99% of occurrences) are shown.

Interaction with time in the models, PCESM

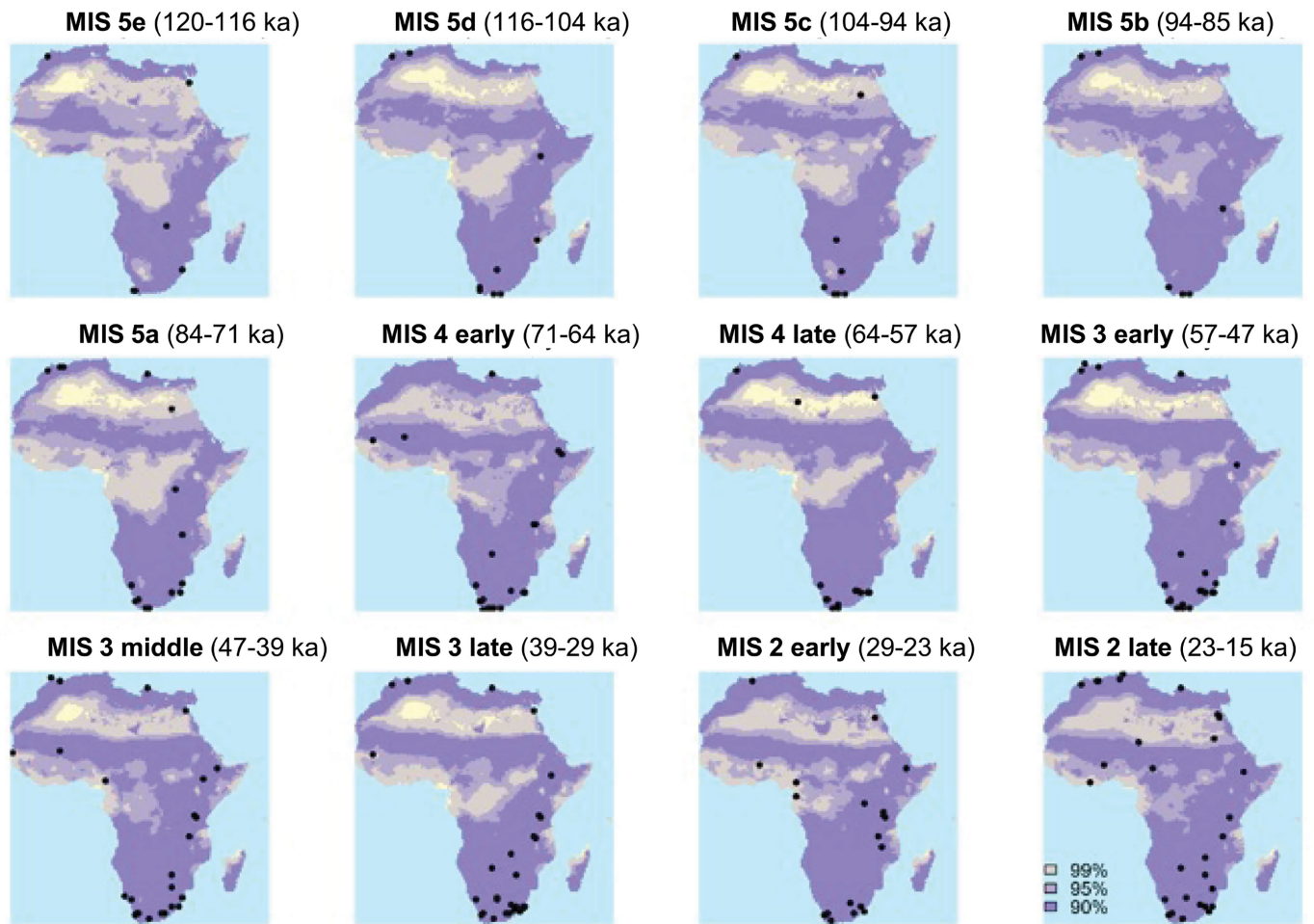


Extended Data Fig. 9 | See next page for caption.

Extended Data Fig. 9 | Interaction with time in the models built using the PCESM^{68,59} climatic simulations. *Homo sapiens* resampled occurrences are shown as grey dots (overlapping points are shown in darker shades based on their number). The partial effects of the GAMs (z axis, colour shading) show the interaction between the variable of interest (y axis) and time (x axis). Here we present the mean values of the partial effects plots over 100 repeats. The red

shading represents favourable variable space (used more than expected by chance given the availability in the whole continent) and blue represents less favourable variable space. The variables used in the GAMs are: temperature annual range (BIO 7), mean temperature of the wettest quarter (BIO 8), mean temperature of the warmest quarter (BIO 10), precipitation of the wettest quarter (BIO 16) and LAI.

Projection fixed-niche model, PCESM



Extended Data Fig. 10 | Projection of the fixed-niche model through time (using climate simulations from PCESM^{58,59}). The core (90% of occurrences), peripheral (95% of occurrences) and total area (99% of occurrences).

Reporting Summary

Nature Portfolio wishes to improve the reproducibility of the work that we publish. This form provides structure for consistency and transparency in reporting. For further information on Nature Portfolio policies, see our [Editorial Policies](#) and the [Editorial Policy Checklist](#).

Statistics

For all statistical analyses, confirm that the following items are present in the figure legend, table legend, main text, or Methods section.

- | | |
|-------------------------------------|--|
| n/a | Confirmed |
| <input type="checkbox"/> | <input checked="" type="checkbox"/> The exact sample size (<i>n</i>) for each experimental group/condition, given as a discrete number and unit of measurement |
| <input type="checkbox"/> | <input checked="" type="checkbox"/> A statement on whether measurements were taken from distinct samples or whether the same sample was measured repeatedly |
| <input type="checkbox"/> | <input checked="" type="checkbox"/> The statistical test(s) used AND whether they are one- or two-sided
<i>Only common tests should be described solely by name; describe more complex techniques in the Methods section.</i> |
| <input type="checkbox"/> | <input checked="" type="checkbox"/> A description of all covariates tested |
| <input type="checkbox"/> | <input checked="" type="checkbox"/> A description of any assumptions or corrections, such as tests of normality and adjustment for multiple comparisons |
| <input type="checkbox"/> | <input checked="" type="checkbox"/> A full description of the statistical parameters including central tendency (e.g. means) or other basic estimates (e.g. regression coefficient) AND variation (e.g. standard deviation) or associated estimates of uncertainty (e.g. confidence intervals) |
| <input type="checkbox"/> | <input checked="" type="checkbox"/> For null hypothesis testing, the test statistic (e.g. <i>F</i> , <i>t</i> , <i>r</i>) with confidence intervals, effect sizes, degrees of freedom and <i>P</i> value noted
<i>Give P values as exact values whenever suitable.</i> |
| <input checked="" type="checkbox"/> | <input type="checkbox"/> For Bayesian analysis, information on the choice of priors and Markov chain Monte Carlo settings |
| <input type="checkbox"/> | <input checked="" type="checkbox"/> For hierarchical and complex designs, identification of the appropriate level for tests and full reporting of outcomes |
| <input type="checkbox"/> | <input checked="" type="checkbox"/> Estimates of effect sizes (e.g. Cohen's <i>d</i> , Pearson's <i>r</i>), indicating how they were calculated |

Our web collection on [statistics for biologists](#) contains articles on many of the points above.

Software and code

Policy information about [availability of computer code](#)

Data collection	No software was used for data collection.
Data analysis	<p>Custom code to perform all analyses in this study was written in R software and is archived and available at the following links: script 1: https://figshare.com/s/d7de3f42aa9e2423bfb5 script 2: https://figshare.com/s/291f499a2b7907dfb62b scripts s01 to s16: https://figshare.com/s/3570c73e7a1d6a5e783e</p> <p>Data analysis was performed using the following software version numbers: QGIS: 3.22 Białowieża Adobe Illustrator: 2025 Adobe Photoshop: 2023 R software: 4.2 rcarbon: 1.4.3 tidysdm: 0.9 pastclim: 1.2 mgcv: 1.9.0 DHARMA: 0.4.6 ecospat: 4.0 gratia: 0.7.3</p>

For manuscripts utilizing custom algorithms or software that are central to the research but not yet described in published literature, software must be made available to editors and reviewers. We strongly encourage code deposition in a community repository (e.g. GitHub). See the Nature Portfolio [guidelines for submitting code & software](#) for further information.

Data

Policy information about [availability of data](#)

All manuscripts must include a [data availability statement](#). This statement should provide the following information, where applicable:

- Accession codes, unique identifiers, or web links for publicly available datasets
- A description of any restrictions on data availability
- For clinical datasets or third party data, please ensure that the statement adheres to our [policy](#)

Climate data extracted from: Beyer, R. M., Krapp, M. & Manica, A. High-resolution terrestrial climate, bioclimate and vegetation for the last 120,000 years. *Scientific Data* 7, 236 (2020). <https://doi.org/10.1038/s41597-020-0552-1>; Yun, K. S. et al. A transient coupled general circulation model (CGCM) simulation of the past 3 million years. *Clim. Past* 19, 1951-1974 (2023). <https://doi.org/10.5194/cp-19-1951-2023>; Zeller, E. et al. Human adaptation to diverse biomes over the past 3 million years. *Science* 380, 604-608 (2023). <https://doi.org/10.1126/science.abq1288>

Archaeological site data from: ROCEEH Out of Africa Database (ROAD) as published in Kandel, A. W. et al. The ROCEEH Out of Africa Database (ROAD): A large-scale research database serves as an indispensable tool for human evolutionary studies. *PLoS One* 18, e0289513 (2023). <https://doi.org/10.1371/journal.pone.0289513>

All archaeological data included in this study is cited and provided within the Supplementary Information. All palaeoclimate data included in this study is cited and provided within the Supplementary Information. Palaeoclimate data is archived and available here: <https://figshare.com/s/2c4253ae6d69d37268a8>

Research involving human participants, their data, or biological material

Policy information about studies with [human participants or human data](#). See also policy information about [sex, gender \(identity/presentation\), and sexual orientation](#) and [race, ethnicity and racism](#).

Reporting on sex and gender	No human participants, their data, or biological material were used in this study.
Reporting on race, ethnicity, or other socially relevant groupings	No human participants, their data, or biological material were used in this study.
Population characteristics	No human participants, their data, or biological material were used in this study.
Recruitment	No human participants, their data, or biological material were used in this study.
Ethics oversight	No human participants, their data, or biological material were used in this study.

Note that full information on the approval of the study protocol must also be provided in the manuscript.

Field-specific reporting

Please select the one below that is the best fit for your research. If you are not sure, read the appropriate sections before making your selection.

☐ Life sciences ☐ Behavioural & social sciences ☒ Ecological, evolutionary & environmental sciences

For a reference copy of the document with all sections, see nature.com/documents/nr-reporting-summary-flat.pdf

Ecological, evolutionary & environmental sciences study design

All studies must disclose on these points even when the disclosure is negative.

Study description	We assembled a comprehensive and curated database of chronometrically dated Pleistocene archaeological sites in Africa and used a species distribution modelling approach to measure changes in the niche breadth of Pleistocene humans in Africa.
Research sample	The coordinates and ages of archaeological sites and layers were recorded from: 1) the existing dataset in ROCEEH Out of Africa Database (ROAD), and 2) published literature, as discussed in Methods.
Sampling strategy	All published archaeological literature was included whenever possible. To account for sampling bias and differential preservation and fieldwork in the archaeological record, we note that each radiometric date is associated with a specific chronological uncertainty, expressed as a range (most likely date and plus/minus). To take into account such uncertainty, we performed our analyses as follows. We created 100 independent datasets: for each of them, the spatial coordinates of all occurrences (=radiometrically dated archaeological layer) were associated to an age that was resampled from the whole chronological range of the date. Such sampling was performed following a truncated normal distribution identified by the mean and the plus/minus as 2-sigma.
Data collection	Archaeological sites and deposits were compiled from peer-reviewed journals and books published before May 5, 2021. The Role of Culture in Early Expansions of Humans (ROCEEH) has been integrating archaeological, paleoanthropological, paleontological and paleobotanical information into the ROCEEH Out of Africa Database (ROAD) since 2009. As of May 2021, the team has compiled information on more than 2000 localities and over 12,000 assemblages in Africa and Eurasia dated between three million and 20,000

years before present. The information in ROAD is structured into localities (sites) with dated layers that contain assemblages of finds including artifacts, human fossils, paleofauna and plant remains as well as bibliographic sources. For this study, AWK and MW queried ROAD to create a list of archaeological localities in Africa dating between ca. 500,000 and 10,000 years and reviewed the output for accuracy. The output also included the ages of the layers as well as radiometric dating results for calibration. For West Africa, JNC collected additional archaeological site data. For North Africa, EYH collected additional archaeological site data.

Timing and spatial scale	Data collection included archaeological site location and dating information for Pleistocene sites in Africa dated to 120,000-14,000 years ago. The ROCEEH Out of Africa Database (ROAD) has been compiling data since 2009. Data collection for this research includes information from peer-reviewed journals and books published before May 5, 2021.
Data exclusions	Exclusion criteria were pre-established. Archaeological sites and layers included in this study met the following pre-established criteria: 1) published coordinates, 2) radiometric dates, 3) an age error range less than or equal to 20,000 years, and 4) mean age $\leq 120,000 \geq 14,000$ years.
Reproducibility	All attempts to repeat the models were successful and all data and code necessary to reproduce the study are provided.
Randomization	We resampled each date 100 times from the truncated normal distribution identified by the mean and the plus/minus as 2-sigma. At the same time, to reduce the conservation bias leading to more recent layers being more frequent, each of those resampled datasets was randomly subsampled to generate a homogeneous distribution in the number of occurrences available through time (thus giving us constant sampling effort through time). For each resampling, we then subset each time slice from the more recent period to the number of occurrences observed in a randomly sampled older slice. To adequately represent the existing climatic space (i.e. background) in our SDMs, each of these resulting datasets was coupled with a random sampling, for each observation, of 200 random locations matched by time. This resulted in n=100 datasets (=“repeats”) of differently sampled and dated presences and differently sampled background points which we used to repeat our analyses to account for the stochastic sampling performed.
Blinding	Blinding was not used during data acquisition or analysis. We assembled a comprehensive database of archaeological site information and do not report experimental results.

Did the study involve field work? ☐ Yes ☒ No

Reporting for specific materials, systems and methods

We require information from authors about some types of materials, experimental systems and methods used in many studies. Here, indicate whether each material, system or method listed is relevant to your study. If you are not sure if a list item applies to your research, read the appropriate section before selecting a response.

Materials & experimental systems

n/a	Involved in the study
<input checked="" type="checkbox"/>	<input type="checkbox"/> Antibodies
<input checked="" type="checkbox"/>	<input type="checkbox"/> Eukaryotic cell lines
<input type="checkbox"/>	<input checked="" type="checkbox"/> Palaeontology and archaeology
<input checked="" type="checkbox"/>	<input type="checkbox"/> Animals and other organisms
<input checked="" type="checkbox"/>	<input type="checkbox"/> Clinical data
<input checked="" type="checkbox"/>	<input type="checkbox"/> Dual use research of concern
<input checked="" type="checkbox"/>	<input type="checkbox"/> Plants

Methods

n/a	Involved in the study
<input checked="" type="checkbox"/>	<input type="checkbox"/> ChIP-seq
<input checked="" type="checkbox"/>	<input type="checkbox"/> Flow cytometry
<input checked="" type="checkbox"/>	<input type="checkbox"/> MRI-based neuroimaging

Palaeontology and Archaeology

Specimen provenance	No specimens were collected.
Specimen deposition	No specimens were collected.
Dating methods	No new dates are provided.
<input checked="" type="checkbox"/>	Tick this box to confirm that the raw and calibrated dates are available in the paper or in Supplementary Information.
Ethics oversight	No ethical approval or guidance was required as no archaeological materials were collected in this study.

Note that full information on the approval of the study protocol must also be provided in the manuscript.

Plants

Seed stocks

n/a

Novel plant genotypes

n/a

Authentication

n/a